

17161

NACA TN 3816

0066708



TECH LIBRARY KAFB, NM

NATIONAL ADVISORY COMMITTEE FOR AERONAUTICS

TECHNICAL NOTE 3816

STATIC STRENGTH OF ALUMINUM-ALLOY SPECIMENS

CONTAINING FATIGUE CRACKS

By Arthur J. McEvily, Jr., Walter Illg,
and Herbert F. Hardrath

Langley Aeronautical Laboratory
Langley Field, Va.



Washington

October 1956

AFMDC

TECHNICAL LIBRARY
OCT 2011



0066708

NATIONAL ADVISORY COMMITTEE FOR AERONAUT.

TECHNICAL NOTE 3816

STATIC STRENGTH OF ALUMINUM-ALLOY SPECIMENS

CONTAINING FATIGUE CRACKS¹

By Arthur J. McEvily, Jr., Walter Illg,
and Herbert F. Hardrath

SUMMARY

Seven configurations of specimens made of 2024 and 7075 aluminum alloys in both rolled and extruded form were subjected to repeated axial loads until fatigue cracks of various lengths were formed. The specimens were then subjected to static tests to determine the residual static strength. Small cracks resulted in disproportionately large reductions of static strength, the reduction being greater for 7075 than for 2024 aluminum alloy. A simple method of analysis which predicts the observed results is developed and described.

INTRODUCTION

The high effective stresses occurring in modern aircraft structures and the nonexistence of the endurance limit for the aluminum alloys from which the structures are built preclude any hope for infinite life. Since fatigue cracks are practically inevitable, the designer and the operator require information regarding the remaining strength of parts containing such cracks. The literature contains very little information on properties of aircraft structural parts containing fatigue cracks. In general, the available information indicates that a very large loss of static strength may be expected in some cases.

In order to supply more of such information, the Langley Laboratory of the NACA has begun a systematic study of the effects of fatigue cracks on the static strength of simple specimens. Tests have been conducted on several configurations of specimens made of 2024 and 7075 aluminum alloys in both rolled and extruded forms.

¹Supersedes NACA Research Memorandum L55D15a by Walter Illg and Herbert F. Hardrath, 1955.

The first part of this paper presents the results of the experimental investigation. Comparisons between characteristics of the materials and specimen configurations are made. The second part of the paper presents a simple method of analysis which was developed to predict the static strength of specimens containing fatigue cracks. The method is based upon calculation of the maximum local stress in the specimen. The elastic stress concentration factor for the configuration is computed according to the theory of elasticity. The elastic factor is then modified for size and plasticity effects according to methods proposed by Neuber (ref. 1) and Stowell (ref. 2). The required material constants were determined experimentally or adjusted empirically.

Appendix A outlines the details of computing stress concentration factors for configurations for which no straightforward solution exists. Appendix B discusses the appearance of the failure surfaces of the specimens.

SYMBOLS

a	half-width of net section, in.
A	area of net section, sq in.
A_0	minimum cross-sectional area of specimen without fatigue cracks or saw cuts, sq in.
e	eccentricity, in.
E	Young's modulus, ksi
E_{sec}	secant modulus, ksi
$(E_s)_\infty$	secant modulus for material remote from hole, ksi
E_u	secant modulus corresponding to point of maximum stress on stress-strain curve, ksi
E_n	secant modulus for nominal stress on net section, ksi
I	moment of inertia, in. ⁴
K_D	elastic stress concentration factor for a deep notch
K_S	elastic stress concentration factor for a shallow notch

K_T	elastic stress concentration factor for a notch of arbitrary depth
K_N	Neuber "engineering" stress concentration factor
K_P	plastic stress concentration factor
K_u	stress concentration factor for ultimate tensile strength
M	moment, in-lb
P	axial load, lb
R	load ratio, $\frac{\text{Minimum load}}{\text{Maximum load}}$
S	nominal stress on net section, ksi
S_O	maximum load divided by A_O , ksi
S_u	ultimate tensile strength of material, ksi
t	depth of notch or crack, or half-length of internal notch, in.
ρ	radius of curvature, in.
ρ_e	effective radius of curvature, in.
ρ'	Neuber material constant, in.
ρ_u	Neuber material constant for ultimate tensile strength, in.
σ_{\max}	maximum local stress, ksi
ω	included angle in notch, radians

EXPERIMENTS

Description of Specimens

Configuration.- Seven configurations of specimens made from two aluminum alloys were tested in this investigation and are as follows:

Specimen		Figure	Material		
Size	Type of notch		Aluminum alloy	Form	Size
$2\frac{7}{4}$ inches wide	Edge notch	1	2024-T3 2024-T4 7075-T6 7075-T6	Sheet Extruded H Sheet Extruded Z	0.081 and 0.090 inch thick 0.125 inch thick 0.090 inch thick 0.102 and 0.125 inch thick
12 inches wide	Edge notch	2	2024-T3 7075-T6	Sheet Sheet	0.081 inch thick 0.075 and 0.081 inch thick
12 inches wide	1-inch hole	2	2024-T3 7075-T6	Sheet Sheet	0.081 inch thick 0.075 inch thick
35 inches wide	1-inch hole		2024-T3 7075-T6	Sheet Sheet	0.102 inch thick 0.102 inch thick
$\frac{3}{4}$ inch thick by 2 inches wide	$\frac{1}{4}$ -inch hole	3	2024-T4 7075-T6	Rolled bar Extruded bar	$\frac{3}{4}$ inch thick by 6 inches wide $\frac{3}{4}$ inch thick by 6 inches wide
$\frac{3}{4}$ inch thick by 4 inches wide	$\frac{1}{8}$ -inch tangs with $\frac{1}{4}$ -inch holes	3	2024-T4 7075-T6	Rolled bar Extruded bar	$\frac{3}{4}$ inch thick by 6 inches wide $\frac{3}{4}$ inch thick by 6 inches wide
$\frac{3}{4}$ inch thick by 4 inches wide	$\frac{1}{4}$ -inch tangs with $\frac{1}{4}$ -inch holes	3	2024-T4 7075-T6	Rolled bar Extruded bar	$\frac{3}{4}$ inch thick by 6 inches wide $\frac{3}{4}$ inch thick by 6 inches wide

In all cases, the faces of the specimens were left as received. The notches were cut by normal machining techniques with no special effort to minimize work hardening. The longitudinal axis of each specimen was parallel to the grain direction.

Material.- Tensile specimens were prepared according to the standards presented in reference 3 from each of the sheets and bars used in this investigation. Tensile tests were performed in the usual manner using autographic stress-strain recording equipment. Dial-gage extensometers were used to measure strains larger than those accommodated by the autographic equipment. The tensile properties thus obtained are summarized in table I. Typical stress-strain curves for each material are given in figure 4. The properties measured indicate that the materials were at least as strong as the minimum values listed in reference 4.

The photomicrographs shown in figure 5 were made of the material used for the small specimens shown in figure 1. The photomicrographs

indicate a normal and uniform grain structure for the sheet materials. The 2024-T4 extruded material shows considerably larger grain size with some tendency for grains to be very long in the longitudinal direction. No indication of grain boundaries was found for the 7075-T6 extruded material even though it was subjected to several different etching agents.

Testing Procedure

$2\frac{1}{4}$ -inch-wide specimens.- The small specimens (fig. 1) were subjected to repeated tension loads in 20,000-pound-capacity subresonant fatigue testing machines. (See ref. 5.) The speed of load application was 1,800 cpm and the initial nominal stress varied between approximately 5 and 30 ksi. Fatigue-crack detector wires (ref. 6) were applied across the critical section of the specimen at intervals of approximately 0.1 inch. The wires nearest the bases of the notches were connected in series with the coil of a relay which stopped the machine when one of the wires failed. Whenever cracks of greater length were desired, the next wire was connected to the stopping circuit and the machine was restarted with the load amplitude arbitrarily reduced by one-half in order to control the rate of crack growth and to prevent failures due to fatigue action alone. This process was repeated with the load amplitude reduced each time until a crack of the desired length had formed. In most cases, approximately 100,000 cycles of load were required to initiate the fatigue crack. In nearly all cases, only one crack was formed.

The specimens containing fatigue cracks were removed from the fatigue machines and placed under a toolmaker's microscope to measure the length of crack visible on each face. The area of the crack was determined by multiplying the average length by the thickness of the specimen. Each specimen was then subjected to steadily increasing tension load until failure occurred. This test was performed in a 120,000-pound-capacity hydraulic testing machine (ref. 7) equipped with grips similar to those used in the fatigue testing machines (ref. 5). The free length between grips during both the fatigue loading and the static test was $11\frac{1}{2}$ inches.

Since most of the $2\frac{1}{4}$ -inch-wide specimens contained only one fatigue crack, the static load was applied eccentrically with respect to the remaining net section. In order to study the effect of the eccentricity on the strength, some of the specimens were modified prior to static testing to reduce the eccentricity. The modifications were accomplished in two ways: In the first method, a longitudinal strip of material was removed (fig. 6) such that the depth of the crack, measured from the new edge, equaled the depth of the notch on the other side. In the second method, a jeweler's saw was used to make a cut equal in depth to that of the fatigue crack in the opposite notch.

A few specimens were tested with jeweler's saw cuts of equal size on both sides of the specimen. These specimens were tested with no repeated loads applied in order to determine whether saw cuts could be used to simulate fatigue cracks.

12-inch-wide specimens.- The 12-inch-wide sheet specimens shown in figure 2 were subjected to repeated axial loads varying between 0 and 45 ksi in the hydraulic testing machine described in reference 7. The loads were cycled automatically by an air servomechanism which was actuated by limit switches attached to the lower grip of the machine. The average speed of cycling was 8 cpm.

The grips used for these tests were flat plates securely fastened to the head and loading ram of the testing machine. Five 1-inch bolts were used to clamp the specimens in each grip. The portions of the faces of the specimen that were clamped inside the grips were roughened with a multiple-point chisel driven by a small rivet gun. The clamping pressure in the grips forced the roughened surfaces of the specimen to embed into plastic liners placed between the specimen and the grips. This procedure gave uniformly secure clamping over the entire width of the specimen.

As in the case of the smaller specimens, fatigue-crack detector wires stopped the machine automatically at intervals during the test. The load was reduced in increments as the crack grew to the desired depth. Whenever deep cracks were desired, the time required to produce the crack was reduced by making a jeweler's saw cut before the repeated loads were applied. In these cases, the crack was always extended at least $1/4$ inch by repeated loading.

After the crack had grown to the desired length, the specimens were subjected to static tensile tests without removing them from the grips. The exact length of the fatigue crack was measured after static failure. In each case, the part of the fracture surface produced by fatigue had a lighter color and a smoother texture than the part which was produced by static failure.

In order to establish the behavior of specimens with very sharp, but known, radius of curvature, four auxiliary tests were performed. The specimens for these tests were made from 12-inch by 36-inch sheets like those shown in figure 2, except for the notches. One specimen of each material had 60° V-notches 2 inches deep on each edge. The root radius was 0.005 inch which gave a theoretical stress concentration factor of 27. (See ref. 1.) Another specimen of each material had notches with parallel sides. A jeweler's saw was used to produce a cut $1\frac{1}{4}$ inches deep. A fine thread coated with valve grinding compound was then used to extend this cut to a depth of 2 inches. The thread and grinding compound produced a reasonably round notch root with a 0.005-inch radius. Because

of the gentle action of this procedure, the material surrounding the root of the notch was expected to be fairly free of residual stress.

35-inch-wide specimens.- The 35-inch-wide specimens were subjected to repeated and static loads in the Langley 1,200,000-pound-capacity testing machine. The cycling was done manually and varied between zero and the maximum stress that could be applied without danger of premature failure. The cycling speed was approximately 3 cpm. Because of the greater amount of time required to produce cracks in these specimens, saw cuts were made in most specimens before cyclic loads were applied. However, the crack was always extended at least $1/4$ inch by repeated loading. Cracks shorter than $1/4$ inch were, of course, made without saw cuts.

The grips for these tests were flat plates clamped to the specimens with 31 bolts in each end. Each grip was fastened to the testing machine by a clevis and pin. Since the cracks grew from a central hole and were usually approximately symmetrical, the pin-ended grips should have acted essentially the same as grips restrained against rotation. As in the case of the 12-inch-wide specimens, the gripped ends of the specimens were roughened and plastic liners were used in the grips.

$3/4$ -inch-thick specimens.- Specimens made from $3/4$ -inch-thick bar stock (fig. 3) were tested in the same grips and machine used for tests of 12-inch-wide sheet specimens. These specimens were subjected to repeated loads varying between 40-ksi tension and 30-ksi compression. Reversed loads were applied to these specimens to make the cracks grow faster. The column strength of the specimens was great enough to support the compression load without guides.

The maximum tension limit was reduced periodically as the crack grew in order to lessen the chances of premature failure; the compression limit was not reduced. The compression loads tended to produce fretting corrosion products on the surfaces of the fatigue cracks which helped to identify the crack boundary after failure. The contour of the fatigue crack was usually irregular and the area was measured with a planimeter after failure.

As described previously for the 12-inch-wide specimens, saw cuts were made to reduce the time required to make deep cracks. Again, in these cases the cracks were always extended at least $1/4$ inch by the cyclic loading.

Results and Discussion

General observations.- The test results are presented in tables II to VI and are plotted in figures 6 to 14. In the presentation of the

data, the strength of the cracked specimen was defined as the maximum load divided by the area of the original net section. This stress is expressed as a percent of the ultimate tensile strength of the material (as determined in tests of standard tensile specimens) and plotted as the ordinate in these figures. The abscissa is the percentage of the original net area which was lost as a result of fatigue cracks and saw cuts. The diagonal dashed line in each figure represents the strength which would be obtained if no stress concentration were present in a cracked specimen. The theoretical curves in each of the figures are explained in the analysis section.

The results of static tests of specimens with notches or holes but without cracks are plotted as solid test points in each figure. For a given configuration, the strength of these 2024 aluminum-alloy specimens was a smaller percentage of the ultimate tensile strength of the material than was the case for the 7075 aluminum-alloy specimens. The strength of specimens with notches or holes sometimes exceeded the static strength of the material. In these cases, the increase in strength of 7075 specimens was generally greater than that of 2024 specimens.

Small fatigue cracks produced rather large decreases in static strength. Generally, the percentage reduction in strength of the 7075 specimens is more than that of 2024 specimens for all lengths of fatigue cracks.

$2\frac{1}{4}$ -inch-wide specimens.- Examination of data in figures 6 to 9 reveals that for small specimens of a given alloy, there was no significant difference between the behaviors of sheet and extruded material, even though the grain structure was quite different (fig. 5).

Efforts to remove the effects of eccentricity resulted in improved strength in nearly all cases. The effect was, of course, more pronounced for specimens containing large cracks where the eccentricity was greatest. In each of the materials, the two methods of reducing the eccentricity (that is, removal of material from the cracked side or making a saw cut on the opposite side) produced similar results.

Tests of specimens with double saw cuts resulted in strengths slightly higher than tests of fatigue-cracked specimens with eccentricity removed. The number of tests may be too small to justify a definite conclusion, but the result was consistent for the cases investigated.

12-inch-wide specimens.- The results of tests on sheet specimens 12 inches wide (fig. 10) indicated a significantly greater reduction in static strength for a given percentage of net area lost by fatigue cracking than did results of tests on smaller specimens. For 7075-T6 aluminum alloy, the strength of specimens with edge notches was affected more by cracks than

was the strength of specimens with central holes. The eccentricity introduced by two cracks of unequal length was evidently more important in specimens with edge notches. This same eccentricity also affected the rates of propagation of the fatigue cracks with the result that the two cracks in a given specimen with edge notches were not likely to be equal in length.

35-inch-wide specimens.- For the configurations tested, the reduction in static strength due to fatigue cracks penetrating a given percentage of the original net area was greatest for the 35-inch-wide sheet specimens (fig. 11). In the worst case, a 7075-T6 specimen with 23.3 percent of its cross section failed experienced a loss of 81.4 percent of the static strength of the material. This loss is equivalent to a stress concentration factor of 5.4 based on original net area or 4.2 based on remaining net area.

When specimens with large fatigue cracks were tested statically, the middle of the specimen tended to buckle out of the plane of the sheet. This buckling was presumably due to the transverse compression forces commonly found near holes at the ends of the diameter parallel to the applied force. In an effort to investigate the importance of this buckling, guides made of wood were applied to one specimen of each of the two materials. This resulted in approximately 25 percent increase in strength in each case. (See fig. 11.)

3/4-inch-thick specimens.- Among the configurations tested, the 3/4-inch-thick specimens with central holes experienced the smallest reduction in static strength due to a given percentage loss of net area. (See fig. 12.) The superior strength can probably be attributed to two factors: First, these specimens were the narrowest specimens tested and, second, the cracks usually grew practically symmetrically from the center. Eccentricities which caused greater reductions in strengths for other configurations were not present to any significant extent in these specimens.

The least consistent set of data was obtained from tests of specimens with tangs. (See table V and figs. 13 and 14.) In these specimens, cracks grew in two directions from each of two holes with the result that the amount of eccentricity present varied erratically from specimen to specimen. In some cases, the crack was encouraged by saw cuts to grow on one side only in an attempt to produce the most eccentric case possible for this configuration. The two different thicknesses of tangs contributed two different percentage losses in net area for a given crack length.

Static failure in all cases but three was sudden when the maximum load was reached. The three specimens not conforming to the normal behavior failed in two stages. One of the tangs failed suddenly at a load somewhat lower than that which finally caused failure of the entire specimen. Both loads were recorded and are indicated in table V(d). The higher

of the two loads was greater than appeared consistent with the test results for other specimens of this type and was not plotted in figures 13 and 14.

ANALYSIS

As shown by the experimental results, the residual static strength of a specimen containing a fatigue crack may vary considerably, depending upon the type of specimen, the extent of the crack, and the material. The purpose of this section is to establish an analytical procedure for the determination of the residual strength of specimens containing fatigue cracks and thereby to eliminate the need for much of the testing which would be required to obtain the information experimentally.

A vast amount of research on failure of structures containing cracks has been conducted in connection with failures in ships and other steel structures. Most of this work indicates that the phenomenon of the transition temperature is involved in the steel problem. Since the aluminum alloys do not exhibit a transition temperature, little of the work on steels can be extended to the study of static strength of aluminum-alloy specimens containing cracks. Irwin (ref. 8) has developed an analysis method involving computation of the elastic energy available to extend a crack and has suggested its application to "brittle" failure in aluminum in addition to steels. Irwin's analysis was developed to predict the load required to cause a sudden failure in a plate containing a slow-running crack.

The results of the present work could not be compared readily with Irwin's theory because sufficiently accurate solutions for the stress distributions in many of the configurations were not available. Furthermore, in the present tests, only the maximum load carried by a given specimen and the length of the crack prior to static loading were recorded. Any extension of the crack during static loading was, therefore, not observed and direct comparison with Irwin's analysis is not possible. The applied load in many tests produced plastic stresses throughout the specimen; thus, elastic analyses are probably not directly applicable.

The point of view adopted in the present paper is that the determination of the residual static strength of a specimen containing a fatigue crack hinges on the determination of the maximum stress in the specimen. The residual static strength of the specimen can then be determined if it is assumed that failure occurs whenever the maximum stress equals the ultimate tensile strength of the material. In view of other work on fracture, the maximum-stress criterion of failure appears to be reasonable (ref. 9) for ductile metals. For tests of sheet specimens, the effects of triaxiality are small and are therefore neglected in this analysis. A procedure for the determination of the stress concentration factor at failure K_t has been developed within this general framework.

Method of Determination of K_u

The general plan which has been chosen to compute K_u is made up of three steps. First, the elastic stress concentration factor K_T for the configuration is computed. Then a correction is made for the absolute size of the notch by a method developed by Neuber. (See ref. 1.) Finally, a correction is made to account for a large decrease in stress concentration brought about by plastic action. As shown subsequently, each of these steps involves an empirical adjustment of one of the parameters used in that step. In order to simplify the presentation and to demonstrate the general applicability of the method, the proposed method is developed first for specimens requiring only the plasticity correction. The method is then extended to situations requiring size and plasticity corrections, and finally the case of the specimen containing fatigue cracks is discussed.

Plasticity effects.— Previous work at the Langley Laboratory has led to methods of predicting stress concentration factors in the plastic range. Griffith (ref. 10) tested 2024-T3 sheet specimens with central holes to study the plastic stress concentration factor for this configuration. Stowell (ref. 2) developed the following expression which agreed well with Griffith's results:

$$K_p = 1 + 2 \frac{E_{sec}}{(E_s)_\infty} \quad (1)$$

where K_p is the stress concentration factor in the plastic range, E_{sec} is the secant modulus for the material at the point of maximum stress, and $(E_s)_\infty$ is the secant modulus for the material remote from the hole.

More recently Budiansky and Vidensek (ref. 11) have analyzed this same problem in a more rigorous manner and have found good agreement between their results and Stowell's, at least for materials like the aluminum alloys.

In an extension of this work, Hardrath and Ohman (ref. 12) tested other configurations of specimens and found that the following generalized form of Stowell's equation yielded satisfactory results:

$$K_p = 1 + \left(K_T - 1 \right) \frac{E_{sec}}{E_n} \quad (2)$$

Although this equation has not been checked by rigorous mathematical analysis nor for large strains, it was tried in the present analysis

because of its simplicity. For calculation of the stress concentration factor at fracture, E_{sec} was replaced by E_u , the secant modulus corresponding to the point of maximum stress on the stress-strain curve. (See fig. 4.) The following expression was thereby obtained:

$$\frac{S_u}{S} = K_u = 1 + (K_T - 1) \frac{E_u}{E_n} \quad (3)$$

The complete stress-strain curve for the material is needed to solve equation (3) for those cases where the applied stress is plastic. In order to simplify the calculations, the secant modulus corresponding to the nominal stress on the net section has been substituted for the secant modulus for material remote from the hole as used by Stowell in reference 2. (This causes no discrepancy with Stowell's analysis because he worked with a hole in an infinite sheet where gross-section stresses and net-section stresses are equal.) Calculations based on equation (3) require a trial-and-error procedure unless the equation is rewritten in the form

$$K_T = 1 + \left(\frac{S_u}{S} - 1 \right) \frac{E_n}{E_u} \quad (4)$$

In order to use this equation, a series of arbitrary values of the failing stress S is assumed. The corresponding values of E_n are found from the stress-strain curve and, since S_u and E_u are constants for the material, a series of K_T values is computed. When these values of K_T are plotted against S_u/S or K_u , the resulting curve may be used to obtain the solution of equation (3) for all values of K_T .

Size effect.— Many investigators working with stress concentration factors have encountered a lack of agreement between values of K_T determined by the theory of elasticity and values determined experimentally. The observed values are always below the theoretical values, the difference increasing with decreasing radius of curvature in the notch. The effect is found most frequently in analysis of fatigue test results.

A relation originally developed by Neuber (ref. 1) has been used by Kuhn and Hardrath (ref. 13) to predict the endurance limits in fatigue tests of steel specimens having notches. The Neuber "engineering" factor is based on the concept that materials are composed of small "building blocks" of linear dimension ρ' across which the stress is constant. The elimination of the steep stress gradient leads to a reduction in stress concentration factor according to the relation:

$$K_N = 1 + \frac{K_T - 1}{1 + \frac{\pi}{\pi - \omega} \sqrt{\frac{\rho'}{\rho}}} \quad (5)$$

where K_T is the elastic stress concentration factor, ω is the included angle in the notch, and ρ is the radius of curvature at the base of the notch. Since the reduction in stress concentration factor is dependent upon the absolute size of the notch, the expression "size effect" has been used in discussion of the phenomenon.

Other forms for reduced stress concentration factors to account for size have been suggested (refs. 14 and 15), but there appears to be no conclusive method for choosing between them. The Neuber factor was chosen to maintain consistency with previous NACA publications.

The combination of size and plasticity effects can be accounted for by merely substituting the Neuber factor K_N (eq. (5)) for the elastic stress concentration factor in equation (3):

$$K_u = 1 + (K_N - 1) \frac{E_u}{E_n} \quad (6)$$

Equations (5) and (6) were used to determine values of ρ' needed to predict the results of the four auxiliary tests described in the experimental part of this paper. Table VI summarized these results. From a knowledge of the specimen configuration, the values of K_T were computed; the values of K_u were found experimentally; and ρ' was adjusted to satisfy equations (5) and (6). Examination of the values of ρ' in table VI indicates some variability, but inasmuch as the square root of this quantity is used in equation (5), little accuracy is lost if the average value ($\rho' = 0.0036$ inch) is used to predict static failure in the aluminum alloys tested in this investigation. In the interest of simplifying the computations, this value of ρ' has been adopted for the analysis which follows.

In the analysis of the long-life fatigue properties of aluminum-alloy specimens containing notches, Kuhn (ref. 16) has reported that a value of $\rho' = 0.02$ inch gives best agreement. The reason for the disagreement between the two values of ρ' is not known, but it is probably reasonable to expect different values to apply for the different modes of failure. The symbol ρ_u will be used in the subsequent discussion for the special value of ρ' which is used for static failure.

For specimens having large radii of curvature at the base of the notch, the size correction is, of course, small and K_N approaches K_T .

Fatigue cracks.- The problem of predicting the static strength of specimens containing fatigue cracks according to the system outlined in the previous sections depends upon the calculation of K_T for the configuration. The value K_T depends critically upon the radius of curvature at the root of the crack, a dimension not readily measurable by ordinary means. In this analysis, the following approach was adopted: The effective radius of curvature ρ_e was assumed to be a constant independent of the prior history of the specimen and independent of the depth of the crack. Several values of ρ_e were then computed from the results of tests on several types of specimens for which K_T could be computed readily. These computations showed that values of ρ_e of the same magnitude as ρ_u were obtained. The assumption that $\rho_e = \rho_u = 0.0036$ inch made possible a further simplification:

$$K_N = 1 + \frac{1}{2}(K_T - 1) \quad (7)$$

and

$$K_u = 1 + \frac{1}{2}(K_T - 1) \frac{E_u}{E_n} \quad (8)$$

Since the stress concentration factors for some of the configurations involved in this investigation were not available in the literature, semiempirical solutions were used. The detailed methods of computing K_T and K_N for the several configurations tested are summarized in appendix A. The values of K_u were then taken from figure 15 which shows in graphical form the solutions of equation (6) for all configurations and each of the materials tested.

Comparison Between Calculations and Experiments

The method described was used to predict the strengths of all of the configurations tested. The results of the computations are presented as the theoretical curves in figures 6 to 14.

For the unmodified $2\frac{1}{4}$ -inch-wide specimens made of each of the four materials (figs. 6 to 9), the agreement between theory and experiment was very good. In the cases of specimens made symmetrical by removal of material or by making a saw cut on the side opposite the fatigue crack, the analysis again gave good predictions or was conservative.

Figure 10 illustrates that for the 12-inch-wide specimens the predictions were good or conservative. The largest discrepancy on the

conservative side is for the strength of 2024-T3 specimen 20, table III. Examination of this specimen revealed that whereas most cracks grew at right angles to the direction of applied load, the fatigue crack in this specimen grew at 70° to the direction of the applied load. For crack growth of this type, the analysis used would be expected to give conservative results.

The theoretical curves in figure 10 for specimens with central holes were computed on the assumption that the cracks were symmetrical. In those tests where the cracks were not symmetrical, the effect of eccentricity was small. Hence, the agreement between tests and predictions was good. On the other hand, theoretical curves for specimens with edge notches were computed on the assumption that only one crack occurred. The prediction is, therefore, very conservative when compared with the strength of specimen 21 in table III in which symmetrical cracks were formed.

The predictions for 35-inch-wide specimens (fig. 11) were in excellent agreement with the tests. For large cracks, the analysis predicted accurately the strength of specimens restrained against buckling. Specimens which were unrestrained and which buckled probably developed additional secondary stresses which decreased their static strength. This buckling may have been present to some extent in specimens having cracks through 25 percent or 30 percent of the original net area.

For $3/4$ -inch-thick specimens (fig. 12) with central holes, the prediction is conservative for 2024-T4 material and unconservative for 7075-T6 material. The assumption that ρ_u was a constant for all the materials used in this investigation may be responsible for this discrepancy. Sheet specimens predominated in this investigation and had a strong influence on the choice of ρ_u . Other values of ρ_u would undoubtedly improve the predictions, but the existing data are probably not sufficient to justify the choice of such new values.

Analysis of the specimens with tangs presents more difficulties than any other case tested. The holes in the tangs tend to produce four cracks, two of which eventually reach the edge of the specimen; thus, the specimen acts thereafter as though it had edge notches. The change in thickness across the width adds additional complications regarding eccentricities and computation of stress concentration factors. Therefore, each specimen should be treated as a separate problem. The curves in figures 13 and 14 were computed according to two simple sets of assumptions to indicate that reasonable estimates can be obtained by the proposed method. In the symmetrical case cracks were considered to grow from both holes, and in the unsymmetrical case cracks were considered to grow from one hole only. These curves are intended to cover the extremes of crack behavior. The details of these computations are outlined in appendix A. Since the actual cracks in many of the specimens did not

conform exactly to either one of these schemes, individual values of the percent material strength were computed and are presented in tables V(b) and V(d) together with the sketches of the corresponding cracked cross sections. When the complexity of the specimen and the assumptions made are considered, the agreement is probably better than would be expected.

In general, the procedure developed herein gives good results, especially for small cracks, which probably are the only ones of real concern. The fact that the method is able to predict differences between behaviors of alloys and types of specimens is considered to be noteworthy.

In addition to simplifying the computation of K_u , figure 15 compares static notch sensitivities of these aluminum alloys. It is seen that the notch sensitivity is a function of K_N . When K_N is large (greater than about 5), the 7075 aluminum alloy is more sensitive to notches than 2024 aluminum alloy because it has a higher ultimate tensile strength and a lower corresponding elongation than does the 2024 material. Therefore, the resulting value for E_u/E_n is greater in the 7075 material than in the 2024 material.

The curves in figure 15 are linear whenever K_u is sufficiently high to cause the net-section stress to be in the elastic range. Then, E_n is E , and E_u/E is a constant. This situation exists for deep cracks or very sharp machined notches in both alloys and, in the 7075 materials, for milder notches.

For lower values of K_N , the 2024 material is more sensitive than the 7075 material. The primary reason for this sensitivity is that for 2024 material the proportional limit is a smaller percentage of the ultimate tensile strength than it is for 7075 material. The result is that the net-section stress is usually well into the plastic range, the value of E_n is less than E , and the value of E_u/E_n for the 2024 material is greater than the value for the 7075 material. Thus, the value of K_u is greater for the 2024 material than for the 7075 material. This fact explains qualitatively why the 2024 specimens exhibit a greater reduction in static strength due to machined notches than do specimens made of 7075 aluminum alloy. The authors know of no other theory which has predicted greater strength reductions for 2024 specimens than for 7075 specimens with like configuration.

Quantitatively, predictions by this analysis method are conservative when applied to tests of specimens with holes or notches but without cracks. The reason for this is not known. The beneficial effects of triaxiality, which have been neglected in this analysis, should be less for large notches than for sharp cracks. Specimens with large notches would therefore be expected to have lower strength. Statistical

sampling effects should also produce lower strength in specimens with larger volumes of material subjected to high stress. Reasonable changes in ρ_u will probably not suffice to improve the predictions significantly since the size correction (eq. (5)) is not very important for the sizes involved.

The effects of specimen width and of eccentricity noted in the experimental part of the paper are also predicted by the analysis method. Figures 16 and 17 show comparisons between predicted curves for the four configurations of specimens tested in each of the two sheet materials. The tendency for wide specimens to be more sensitive to cracks than narrow specimens is apparent. The curves for 12-inch-wide and 35-inch-wide specimens with central holes tend to be parallel for cracks penetrating more than 10 percent of the original net area. The curves for specimens with edge notches ($2\frac{1}{4}$ and 12 inches wide) are also parallel for cracks penetrating more than 10 percent of the original net area but show considerably more reduction in strength for deep cracks as a result of the eccentricities present than do the curves for specimens with central holes.

The general agreement between theory and experiment tends to justify the assumptions made, at least for the aluminum alloys tested. As yet the method has not been tried for other materials, and the proposed method of determining K_u should not be extended without further checking. However, it is expected that many of the practical problems associated with crack growth in aircraft will concern aluminum structural alloys, for which the present method appears applicable.

CONCLUSIONS

Static tests of 2024 and 7075 aluminum-alloy specimens containing mild machined notches but without cracks revealed that the strength of the 2024 specimens is lower, percentagewise, than is the strength of the 7075 specimens.

Static tests of 2024 and 7075 aluminum-alloy specimens containing fatigue cracks support the following conclusions:

1. Small cracks caused large decreases in static strength.
2. The static strength of specimens made of 7075 aluminum alloy was significantly more sensitive to the effects of cracks than the static strength of similar specimens made of 2024 aluminum alloy.

3. On the basis of percentage of net area lost by fatigue cracking, wide specimens experienced greater loss of strength than narrow specimens with similar configurations.

4. Specimens tested with the final net area eccentric with respect to the load had lower static strengths than similar specimens which were loaded along a line passing through the center of the remaining area.

5. There was little, if any, difference between static strengths of similar specimens made of sheet and extruded material for the same alloy.

A method of analysis based on calculation of an elastic stress concentration factor for the configuration and on corrections for size and plasticity according to the Neuber "engineering" factor and the Stowell formula, respectively, was reasonably successful in predicting the observed test results. Empirical evaluation of the effective radius of curvature at the root of a fatigue crack in the materials tested and of the Neuber constant showed that good agreement was obtained when both quantities were assigned the value 0.0036 inch.

Langley Aeronautical Laboratory,
National Advisory Committee for Aeronautics,
Langley Field, Va., July 6, 1956.

APPENDIX A

DETERMINATION OF K_N

This appendix is a brief outline of the methods of computation used in the main body of the paper for the determination of K_N . In each case the effects of eccentricities, if any, must be accounted for and the combination of a large machined notch and a small crack must be considered. Each type of configuration will be treated.

Central Hole With Small Cracks

Howland's analysis (ref. 17) for a hole in a finite sheet was used to obtain K_T for the hole. This value was corrected for size by the

Neuber formula: $K_N = 1 + \frac{K_T - 1}{1 + \sqrt{\frac{\rho'}{\rho}}}$. Small cracks within the highly stressed

regions beside the hole were assumed to act in a manner similar to that of shallow cracks in a sheet having parallel sides. The formula for shallow notches (ref. 1)

$$K_T \approx K_S = 1 + 2\sqrt{\frac{t}{\rho_u}} \quad (A1)$$

was used. For the case where $t = \rho_u = 0.0036$ inch, this formula yields the value 3 and substitution of this value into equation (7) produces $K_N = 2$. The value of K_N for the combination of a hole and a very small crack was then assumed to be the product of these two values of K_N or, simply, twice the value of K_N for the hole. Figure 15 was then used to obtain the corresponding value of K_u . This method was used to compute one point on each of the predicted curves.

Central Hole With Large Cracks

As the crack becomes larger the stress distribution becomes less dependent upon the existence of the original hole. The configuration was assumed to be represented by an ellipse whose major axis equaled the diameter of the hole plus the crack length. Existing analyses (refs. 1 and 18) of stresses around ellipses in finite sheets are not readily extended to cases in which the ellipse is not in the middle of the specimen.

The following semiempirical method was therefore used to estimate the stresses at cracks originating from a central hole. Neuber (ref. 1) and others have suggested the form

$$K_T = 1 + 2 \sqrt{\frac{t}{\rho}}$$

for a small ellipse in a wide sheet. This formula yields the appropriate value of 3 for the circular hole. If it is assumed that the first term accounts for the stress present without a notch and that the factor $\sqrt{t/\rho}$ accounts for the flatness of the ellipse, appropriate modification of the factor 2 might account for the finite width of the sheet. The Howland and Sjöström analyses (refs. 17 and 19) were used to make this modification as follows:

$$(K_T)_{\text{ellipse}} = 1 + \left[(K_T)_{\text{hole}} - 1 \right] \sqrt{\frac{t}{\rho}} \quad (\text{A2})$$

where $(K_T)_{\text{hole}}$ is the stress concentration factor for a hole with a diameter equal to the major axis of the ellipse and located at the appropriate position in a sheet of finite width (values from fig. 18). This analysis yields values somewhat greater than those predicted by Westergaard (ref. 18), but was used because of the possibility of applying it to eccentric cases.

Values of K_u for cracks with $t/\rho > 10$ were obtained by computing K_T according to the method just described, K_N according to formula (7), and finally K_u from figure 15. In the narrow region $1 < t/\rho < 10$, the predicted strength curve was arbitrarily faired.

Symmetrical Edge Notch With Cracks

The same type of analysis as described in the preceding section was used for small cracks ($t/\rho = 1$). The value of K_N for the edge notch was determined by Neuber's equations for deep and shallow notches, his transition formula

$$K_T = 1 + \frac{(K_S - 1)(K_D - 1)}{\sqrt{(K_S - 1)^2 + (K_D - 1)^2}} \quad (\text{A3})$$

and finally his engineering factor (eq. (7)). This value of K_N was multiplied by 2 which is the value of K_N for a crack with $t/\rho = 1$.

Stress concentration factors for cracks deeper than $t/\rho = 10$ were again assumed to be independent of the original notch. The configuration was then assumed to be represented by symmetrical edge notches whose depth equaled the sum of notch depth and crack depth. Neuber's relations were used as before. Since in each of the cases under consideration the ratios t/ρ and a/ρ are large, the Neuber relations may be simplified by taking the limiting form of each relation as $\rho \rightarrow 0$. This procedure results in

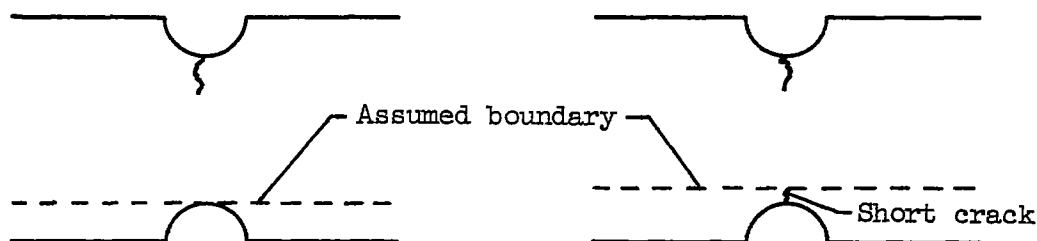
$$K_S = 1 + 2\sqrt{t/\rho} \quad (A4)$$

and

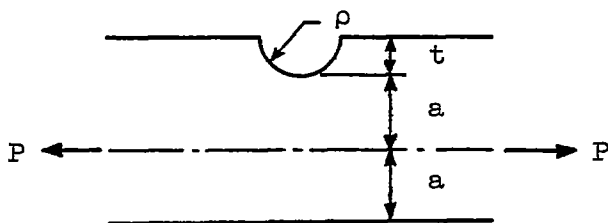
$$K_D = \frac{4}{\pi} \sqrt{a/\rho} \quad (A5)$$

Edge Notches With Unsymmetrical Cracks

In nearly all cases, the cracks in specimens having edge notches were either on one side only or significantly longer on one side than on the other. Trial computations showed that, in each case, the best predictions were obtained when the side of the specimen opposite the longest crack was assumed to have a straight boundary. For example,



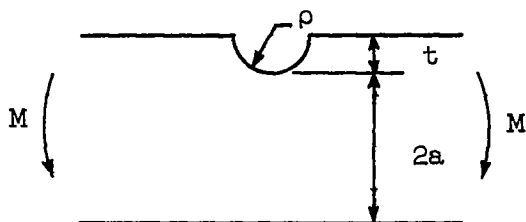
Neuber has two solutions which are useful to treat unsymmetrical cracks. The first is the solution for local stress due to tension load applied along the axis passing through the center of the net section and is shown by the following illustration and equations:



$$K_S = 1 + 2\sqrt{t/\rho} \quad (A6a)$$

$$K_D = 0.83\sqrt{a/\rho} \quad (A6b)$$

The second is for local stress due to bending and is as follows:



$$K_S = 1 + 2\sqrt{t/\rho} \quad (A7a)$$

$$K_D = 1.13\sqrt{a/\rho} \quad (A7b)$$

Both sets of equations (eqs. (A6) and (A7)) were used, and K_T and K_N for the axial load and bending cases were obtained from the usual Neuber relations (eqs. (A3) and (5)). The local stress was finally obtained from the following relation:

$$\sigma_{\max} = \frac{P}{A}(K_N)_{\text{axial}} + \frac{Ma}{I}(K_N)_{\text{bending}} \quad (A8)$$

Based upon some additional tests designed to determine the end fixity of the specimens in the testing machine, the moment M in the above relation was taken to be $\frac{3}{4}Pe$ where e is the eccentricity of the load with respect to the remaining net section. For rectangular cross sections, equation (A8) reduces to

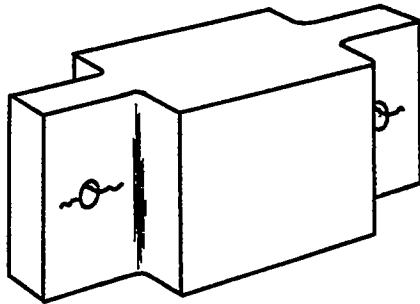
$$(K_N)_{\text{combination}} = \frac{\sigma_{\max}}{P/A} = (K_N)_{\text{axial}} + \frac{9}{4} \frac{e}{a} (K_N)_{\text{bending}} \quad (A9)$$

Equation (A9) was used to compute K_N for all cases of cracks growing from edge notches except for the cases where the specimens were made symmetrical by removal of material or by saw cuts. In these cases, no bending was present and only $(K_N)_{\text{axial}}$ was needed.

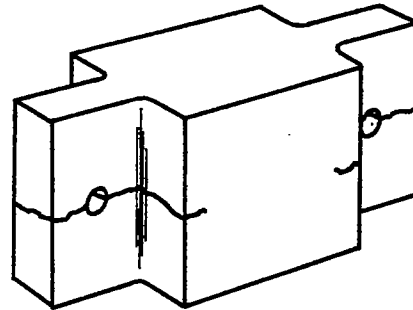
Specimens With Tangs

The theoretical curves for specimens with tangs, figures 13 and 14, were computed for two assumed modes of crack growth: symmetrically cracked and cracked on one side only.

For the symmetrical case, cracks of equal length were assumed to grow as shown:



Case A



Case B

The analysis for case A was similar to that used for holes with cracks in sheet specimens. Case B was analyzed by using the procedure for symmetrical edge notches.

For the case of cracks on one side only, cracks were assumed to grow from one hole instead of both. The analysis was similar to that for the symmetrical case except that the eccentricity of loading was also taken into account.

Since two different thicknesses of tang contributed different percentages of area for a given crack depth, a separate strength curve was found for each. Individual percent material strengths computed for each of the actual crack configurations are presented in tables V(b) and V(d).

APPENDIX B

APPEARANCE OF FAILURE SURFACES

One interesting aspect of the investigation was the appearance of the failure surfaces. In every case the boundary between the fatigue crack and the static failure was clearly visible. The contrast was particularly striking in the cases of the 3/4-inch-thick specimens. Figure 19 shows photographs of typical specimens.

The "herringbone" patterns visible in figure 19(a) were found only in the 2024-T4 specimens with tangs. The static failure of thick specimens without tangs in each of the materials was characterized by a granular surface on a plane normal to the axis of the specimen except for the outer 1/8 inch of material, where the familiar shear failure was present. Failures in 7075-T6 specimens with tangs (fig. 19(c)) were extremely jagged and had little tendency to occur along a plane normal to the axis of the specimen. Some evidence of lamination in the material was found for these latter specimens although specimens without tangs cut from the same bars showed no such characteristics.

Fatigue cracks in the sheet specimens and thin extrusions were usually in a plane normal to the surface. The statically failed portion of the surface was usually of the shear type. However, in 7075-T6 specimens there was a consistent tendency for the material near the middle of the thickness to fail along a surface normal to the face of the sheet. The usual shear failure was present near both faces.

REFERENCES

1. Neuber, Heinz: Theory of Notch Stresses: Principles for Exact Stress Calculation. J. W. Edwards (Ann Arbor, Mich.), 1946.
2. Stowell, Elbridge Z.: Stress and Strain Concentration at a Circular Hole in an Infinite Plate. NACA TN 2073, 1950.
3. Anon.: 1955 Book of ASTM Standards Including Tentatives. Part 2 - Non-Ferrous Metals. Tentative Methods of Tension Testing of Metallic Materials (ASTM Designation: E8-54T). A.S.T.M. (Philadelphia), 1955, pp. 1246-1260.
4. Anon.: Strength of Metal Aircraft Elements. ANC-5, Munitions Board Aircraft Committee, Dept. of Defense. Revised ed., June 1951.
5. Grover, H. J., Hyler, W. S., Kuhn, Paul, Landers, Charles B., and Howell, F. M.: Axial-Load Fatigue Properties of 24S-T and 75S-T Aluminum Alloy As Determined in Several Laboratories. NACA Rep. 1190, 1954. (Supersedes NACA TN 2928.)
6. McGuigan, M. J., Jr., Bryan, D. F., and Whaley, R. E.: Fatigue Investigation of Full-Scale Transport-Airplane Wings - Summary of Constant-Amplitude Tests Through 1953. NACA TN 3190, 1954.
7. Hardrath, Herbert F., and Illg, Walter: Fatigue Tests at Stresses Producing Failure in 2 to 10,000 Cycles - 24S-T3 and 75S-T6 Aluminum-Alloy Sheet Specimens With a Theoretical Stress-Concentration Factor of 4.0 Subjected to Completely Reversed Axial Load. NACA TN 3132, 1954.
8. Irwin, George: Fracture Dynamics. Fracturing of Metals. A.S.M. (Cleveland), c.1948, pp. 147-166.
9. Gensamer, Maxwell: Strength of Metals Under Combined Stresses. American Soc. Metals (Cleveland), c.1941.
10. Griffith, George E.: Experimental Investigation of the Effects of Plastic Flow in a Tension Panel With a Circular Hole. NACA TN 1705, 1948.
11. Budiansky, Bernard, and Vidensek, Robert J.: Analysis of Stresses in the Plastic Range Around a Circular Hole in a Plate Subjected to Uniaxial Tension. NACA TN 3542, 1955.
12. Hardrath, Herbert F., and Ohman, Lachlan: A Study of Elastic and Plastic Stress Concentration Factors Due to Notches and Fillets in Flat Plates. Rep. 1117, 1953. (Supersedes NACA TN 2566.)

13. Kuhn, Paul, and Hardrath, Herbert F.: An Engineering Method for Estimating Notch-Size Effect in Fatigue Tests on Steel. NACA TN 2805, 1952.
14. Heywood, R. B.: Stress Concentration Factors - Relating Theoretical and Practical Factors in Fatigue Loading. Engineering, vol. 179, no. 4645, Feb. 4, 1955, pp. 146-148.
15. Siebel, E., and Stieler, M.: Ungleichförmige Spannungsverteilung bei schwingender Beanspruchung. Z.V.D.I., Bd. 97, Nr. 5, Feb. 11, 1955, pp. 121-126.
16. Kuhn, P.: Effect of Geometric Size on Notch Fatigue. Int. Union of Theor. and Appl. Mech. Colloquium on Fatigue (Stockholm, May 1955), Springer (Berlin), 1956, pp. 131-140.
17. Howland, R. C. J.: On the Stresses in the Neighbourhood of a Circular Hole in a Strip Under Tension. Phil. Trans. Roy. Soc. (London), ser. A, vol. 229, no. 671, Jan. 6, 1930, pp. 49-86.
18. Westergaard, H. M.: Bearing Pressures and Cracks. Jour. Appl. Mech., vol. 6, no. 2, June 1939, pp. A-49 - A-53.
19. Sjöström, S.: On the Stresses at the Edge of an Eccentrically Located Circular Hole in a Strip Under Tension. Rep. No. 36, Aero. Res. Inst. of Sweden (Stockholm), 1950.

TABLE I

TENSILE PROPERTIES OF MATERIALS TESTED

Material	Yield stress (0.2 percent offset), ksi	Ultimate strength, ksi	Total elongation, 2-inch gage length, percent	Young's modulus, ksi	Number of specimens
2024-T3 sheet	52.7	71.9	19.5	10.6×10^3	14
2024-T4 extrusion	52.7	67.2	16.7	10.5	40
2024-T4 rolled bar	46.2	64.8	20.9	10.2	34
7075-T6 sheet	74.0	80.5	12.8	10.3	6
7075-T6 extrusion	78.5	86.6	11.0	10.5	16
7075-T6 extruded bar	77.9	89.0	13.3	10.6	12

TABLE II

RESULTS OF STATIC TESTS OF $\frac{1}{4}$ -INCH-WIDE SPECIMENS

(a) Unmodified specimens

2024-T3 sheet				2024-T4 extrusion				7075-T6 sheet				7075-T6 extrusion			
Specimen	Cracked area, percent original area	Static strength, kai	Static strength, S_0/S_u , percent	Specimen	Cracked area, percent original area	Static strength, kai	Static strength, S_0/S_u , percent	Specimen	Cracked area, percent original area	Static strength, kai	Static strength, S_0/S_u , percent	Specimen	Cracked area, percent original area	Static strength, kai	Static strength, S_0/S_u , percent
1	0.0	73.8	102.6	25	0.0	71.0	105.5	42	0.0	87.3	108.4	66	0.0	87.6	101.2
2	2.0	54.4	75.7	26	6.3	53.3	79.2	43	1.0	76.8	95.5	67	0.0	82.7	95.5
3	4.6	49.6	69.1	27	9.7	45.3	67.4	44	1.8	62.9	78.1	68	0.8	70.8	81.7
4	7.5	49.0	68.2	28	10.3	44.4	66.0	45	2.2	69.8	86.8	69	1.0	49.0	56.5
5	7.5	48.6	67.8	29	15.7	39.0	58.0	46	2.5	55.0	68.4	70	2.1	71.3	82.3
6	12.4	41.1	57.5	30	25.2	30.3	45.0	47	9.6	48.2	60.0	71	5.1	54.4	62.8
7	13.2	46.2	64.4	31	26.5	30.5	45.4	48	13.4	42.3	52.8	72	7.0	50.5	58.3
8	13.9	38.4	53.5	32	27.7	28.0	47.5	49	15.8	40.6	50.5	73	8.6	50.0	57.7
9	15.7	44.3	61.6	33	27.8	31.4	46.7	50	16.0	42.4	52.7	74	11.8	45.5	50.2
10	17.6	43.0	59.9	34	33.0	29.9	44.5	51	18.5	40.5	50.4	75	18.0	36.0	41.6
11	23.3	35.6	49.5	35	33.2	27.6	41.0	52	21.5	38.6	48.0	76	26.6	31.2	36.0
12	24.2	38.9	54.1	36	33.3	26.6	39.6	53	28.4	35.2	43.7	77	27.0	28.4	32.8
13	27.3	33.3	49.1	37	37.2	26.2	39.0	54	31.7	29.2	36.5	78	28.8	30.9	33.7
14	27.6	33.2	46.2	38	43.5	24.8	36.9	55	32.4	31.8	39.5	79	29.0	31.2	36.0
15	29.0	30.3	42.5	39	44.6	22.8	33.9	56	36.9	25.0	31.1	80	29.0	27.9	31.0
16	29.5	33.1	46.0	40	48.4	20.6	30.6	57	37.0	26.4	32.8	81	32.2	30.2	34.8
17	30.5	31.6	44.0	41	75.4	12.5	18.6	58	38.2	27.3	34.0	82	37.5	27.5	31.7
18	30.8	32.8	45.6					59	39.0	24.4	30.4	83	40.2	23.0	26.6
19	33.0	29.4	41.0					60	39.5	25.2	31.3	84	47.2	21.4	24.7
20	34.0	32.5	45.2					61	42.9	23.9	28.2	85	61.1	16.1	18.6
21	39.9	29.0	40.3					62	43.2	23.1	28.7	86	62.6	14.4	16.6
22	42.5	27.0	37.6					63	43.9	20.9	26.0				
23	44.6	24.3	33.8					64	45.8	22.9	28.5				
24	45.9	23.8	33.1					65	53.0	19.9	24.8				

TABLE II.- Continued

RESULTS OF STATIC TESTS OF $\frac{1}{4}$ -INCH-WIDE SPECIMENS

(b) Modified specimens

2024-T3 sheet				2024-T4 extrusion				7075-T6 sheet				7075-T6 extrusion			
Eccentricity reduced (material removed)															
Specimen	Cracked area, percent original area	Static strength, ksi	Static strength, S_u/R_u , percent	Specimen	Cracked area, percent original area	Static strength, ksi	Static strength, S_u/R_u , percent	Specimen	Cracked area, percent original area	Static strength, ksi	Static strength, S_u/R_u , percent	Specimen	Cracked area, percent original area	Static strength, ksi	Static strength, S_u/R_u , percent
1	15.7	46.0	64.0	16	5.3	50.6	75.4	26	3.6	55.0	68.5	49	11.8	52.0	60.0
2	26.2	42.0	58.5	17	30.5	35.8	50.3	27	10.5	54.4	67.5	50	19.9	45.6	50.3
3	32.3	38.3	53.5	18	56.9	25.6	35.1	28	30.6	42.0	52.1	51	39.7	38.9	44.9
4	40.0	34.4	48.0					29	58.2	40.2	50.0				
5	58.4	22.3	31.0					30	46.7	37.8	47.0				
								31	57.5	32.4	40.2				
Eccentricity reduced (saw cut)															
6	7.5	50.6	70.5	19	4.7	54.6	81.3	32	7.2	56.1	69.8	52	14.5	36.7	42.3
7	17.1	46.8	65.0	20	19.7	46.5	69.2	33	15.2	52.0	64.6	53	17.7	30.4	38.1
8	35.6	35.6	49.6	21	65.8	21.0	31.2	34	21.0	49.5	61.5	54	18.3	31.0	38.9
9	43.0	32.5	45.2	22	69.6	20.5	30.5	35	25.0	46.4	70.0	55	29.2	44.9	51.8
10	58.5	24.1	35.6					36	26.0	43.0	55.5	56	35.1	38.9	45.0
								37	54.5	41.0	51.0	57	40.4	39.4	45.5
								38	59.5	42.6	55.0	58	58.0	30.6	35.5
								39	59.8	43.6	54.2				
								40	42.0	42.1	52.4				
								41	44.7	40.8	50.6				
								42	56.4	32.7	40.6				
								43	59.0	29.6	36.8				
Symmetrical saw cuts (no fatigue crack)															
11	6.9	53.7	74.9	23	8.9	52.4	77.9	44	8.6	65.7	81.6	59	10.0	66.5	76.8
12	8.5	53.9	75.0	24	32.7	40.0	59.5	45	15.4	52.7	65.5	60	39.5	51.1	59.1
13	33.8	40.2	56.0	25	55.2	40.3	60.0	46	34.6	48.0	59.6	61	40.0	45.5	50.2
14	65.5	22.9	31.9					47	55.5	34.1	42.4	62	65.9	26.7	30.8
15	66.0	21.1	29.4					48	66.4	27.8	34.6				

TABLE III

RESULTS OF STATIC TESTS OF 12-INCH-WIDE SPECIMENS

2024-T3 sheet								7075-T6 sheet							
With central hole				With edge notch				With central hole				With edge notch			
Specimen	Cracked area, percent original area	Static strength, ksi	Static strength, S_0/S_u , percent	Specimen	Cracked area, percent original area	Static strength, ksi	Static strength, S_0/S_u , percent	Specimen	Cracked area, percent original area	Static strength, ksi	Static strength, S_0/S_u , percent	Specimen	Cracked area, percent original area	Static strength, ksi	Static strength, S_0/S_u , percent
1	0.0	62.1	86.5	14	0.0	69.8	97.1	22	0.0	78.2	97.2	28	0.0	83.4	105.5
2	0.0	58.8	81.9	15	1.1	56.7	79.0	23	0.1	64.0	79.5	29	0.1	65.3	81.1
3	2.5	50.9	70.8	16	11.7	45.4	63.1	24	2.1	49.6	61.7	30	1.3	42.9	53.3
4	3.0	51.7	72.0	17	12.0	41.5	57.8	25	9.3	41.6	51.8	31	2.2	35.0	43.5
5	13.0	43.2	60.2	18	12.6	44.5	61.6	26	18.0	40.7	50.6	32	3.9	39.7	49.3
6	17.4	43.1	54.8	19	23.4	36.4	50.7	27	29.8	23.9	29.1	33	5.8	32.5	40.4
7	17.8	41.4	43.2	20	41.0	28.3	39.4					34	13.6	31.6	39.3
8	18.0	44.3	56.0	21	41.9	31.3	43.5					35	23.7	23.5	31.7
9	19.8	39.7	55.3												
10	34.0	26.8	37.3												
11	34.7	27.9	38.9												
12	34.8	28.8	38.8												
13	35.9	27.6	38.4												

TABLE IV

RESULTS OF STATIC TESTS OF 35-INCH-WIDE SPECIMENS

2024-T3 sheet				7075-T6 sheet			
Specimen	Cracked area, percent original area	Static strength, ksi	Static strength, S_0/S_u , percent	Specimen	Cracked area, percent original area	Static strength, ksi	Static strength, S_0/S_u , percent
1	0.0	57.9	80.5	8	0.0	80.2	99.5
2	0.2	49.6	69.0	9	0.8	46.2	57.5
3	1.4	48.1	66.9	10	4.5	35.6	44.0
4	11.6	37.4	52.0	11	14.7	22.5	27.7
5	28.5	23.6	32.8	12	23.5	15.3	19.0
6	49.5	13.6	18.9	13	49.6	9.8	12.2
7	49.7*	19.1	26.6	14	50.0*	12.0	14.9

*With guides.

TABLE V

RESULTS OF STATIC TESTS OF 3/4-INCH-THICK SPECIMENS

(a) 2024-T4 rolled bar 2 inches wide















Specimen	Crack profile	Cracked area, percent original area	Static strength, ksi	Static strength, S_o/S_u , percent
1		0	58.3	90.0
2		3.8	48.0	74.1
3		4.7	48.7	75.5
4		5.7	46.5	72.1
5		9.0	45.1	69.8
6		10.3	45.0	69.5
7		11.9	42.5	65.7
8		15.0	41.9	64.7
9		15.8	41.6	64.1
10		20.8	39.0	60.3
11		34.0	32.2	49.8
12		36.0	32.0	49.5
13		54.1	24.4	37.7
14		62.0	19.3	29.8

TABLE V.- Continued

RESULTS OF STATIC TESTS OF 3/4-INCH-THICK SPECIMENS

(b) 2024-T4 rolled bar with tangs

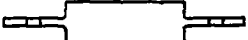




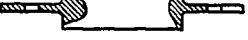

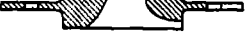

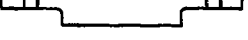
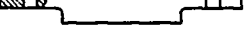



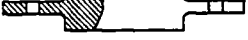
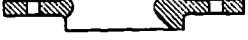

Specimen	Crack profile	Cracked area, percent original area	Static strength, ksi	Static strength, S_0/S_u , percent	
				Experiment	Theory
1		0	54.0	83.5	77.0
2		1.6	47.9	74.0	67.5
3		7.9	44.8	69.3	64.0
4		22.6	31.4	48.5	51.0
5		31.6	34.2	52.9	48.1
6		33.4	37.6	55.6	48.1
7		38.0	24.2	37.4	39.5
8		47.1	25.3	39.0	37.0
9		52.5	19.6	30.2	31.9
10		0	56.6	87.6	77.0
11		8.3	44.4	68.5	63.3
12		8.9	43.1	66.8	66.0
13		19.4	40.9	62.4	56.0
14		19.4	33.0	51.0	54.0
15		29.8	26.2	40.3	45.3
16		37.6	30.2	46.9	44.0
17		51.0	19.1	29.5	26.8

TABLE V.- Continued

RESULTS OF STATIC TESTS OF 3/4-INCH-THICK SPECIMENS

(c) 7075-T6 extrusion 2 inches wide



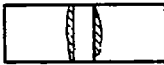





Specimen	Crack profile	Cracked area, percent original area	Static strength, ksi	Static strength, S_o/S_u , percent
1		0	87.9	98.5
2		2.9	64.2	72.0
3		3.2	69.6	73.3
4		8.3	45.9	51.5
5		15.6	38.8	43.5
6		41.9	23.6	25.8
7		42.4	22.2	25.0
8		61.6	16.2	18.2

TABLE V.- Concluded

RESULTS OF STATIC TESTS OF 3/4-INCH-THICK SPECIMENS

(d) 7075-T6 extrusion with tangs

[For specimens 2, 3, and 10, the first numbers indicate the conditions under which the crack advanced completely through one tang. The numbers in parentheses are conditions at final failure of the specimen.]







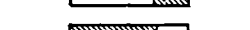
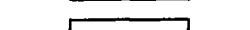
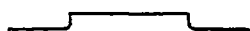
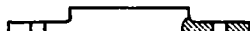




Specimen	Crack profile	Cracked area, percent original area	Static strength, ksi	Static strength, S_c/S_u , percent	
				Experiment	Theory
1		0	82.4	92.5	86.0
2		0.1 (5.6)	72.5 (74.5)	81.3 (83.6)	64.0
3		1.0 (5.6)	67.0 (76.7)	75.1 (86.1)	77.4
4		5.6	71.5	80.3	51.9
5		9.9	69.1	77.8	47.6
6		17.2	38.4	43.1	37.7
7		34.0	21.0	23.6	30.0
8		70.8	7.6	8.5	7.5
9		0	85.4	95.7	86.0
10		1.0 (10.0)	59.5 (67.7)	66.8 (76.0)	77.4
11		11.5	46.5	52.4	42.5
12		18.4	27.6	31.0	34.7
13		27.6	18.0	20.2	29.3
14		46.5	12.3	13.8	19.7

TABLE VI
RESULTS OF AUXILIARY TESTS

$$[\rho = 0.005 \text{ in.}; K_T = 27.4]$$

Aluminum alloy	Type of notch	Experimental K_u	K_N (eq. (5))	Computed ρ' , in.
2024-T3	60° V-notch	1.46	12.5	0.0038
7075-T6	60° V-notch	2.15	15.0	.0019
2024-T3	U-notch	1.48	13.7	.0057
7075-T6	U-notch	2.25	16.2	.0028
				<hr/> Av. = 0.0036

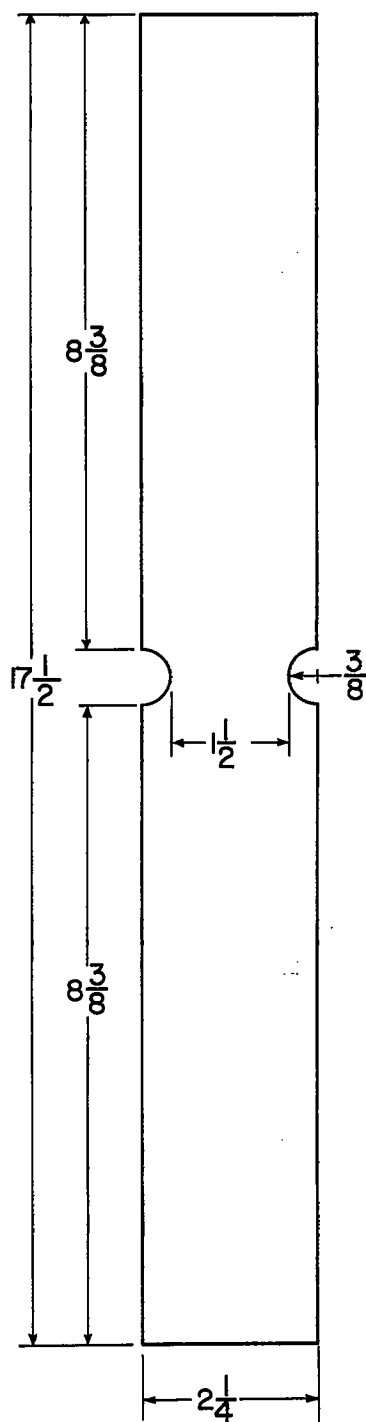


Figure 1.- Configuration of small specimens.

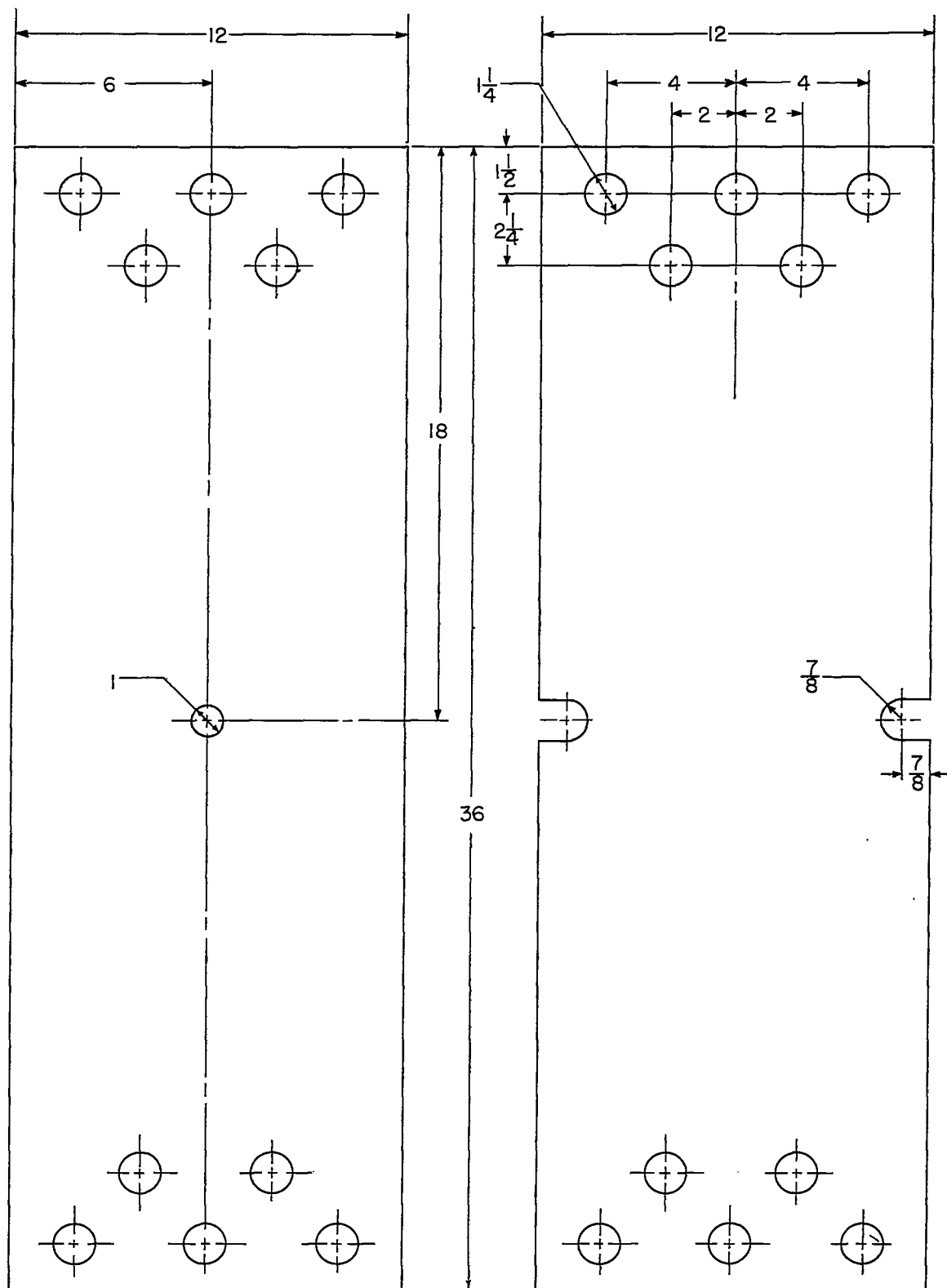


Figure 2.- Configuration of sheet specimens.

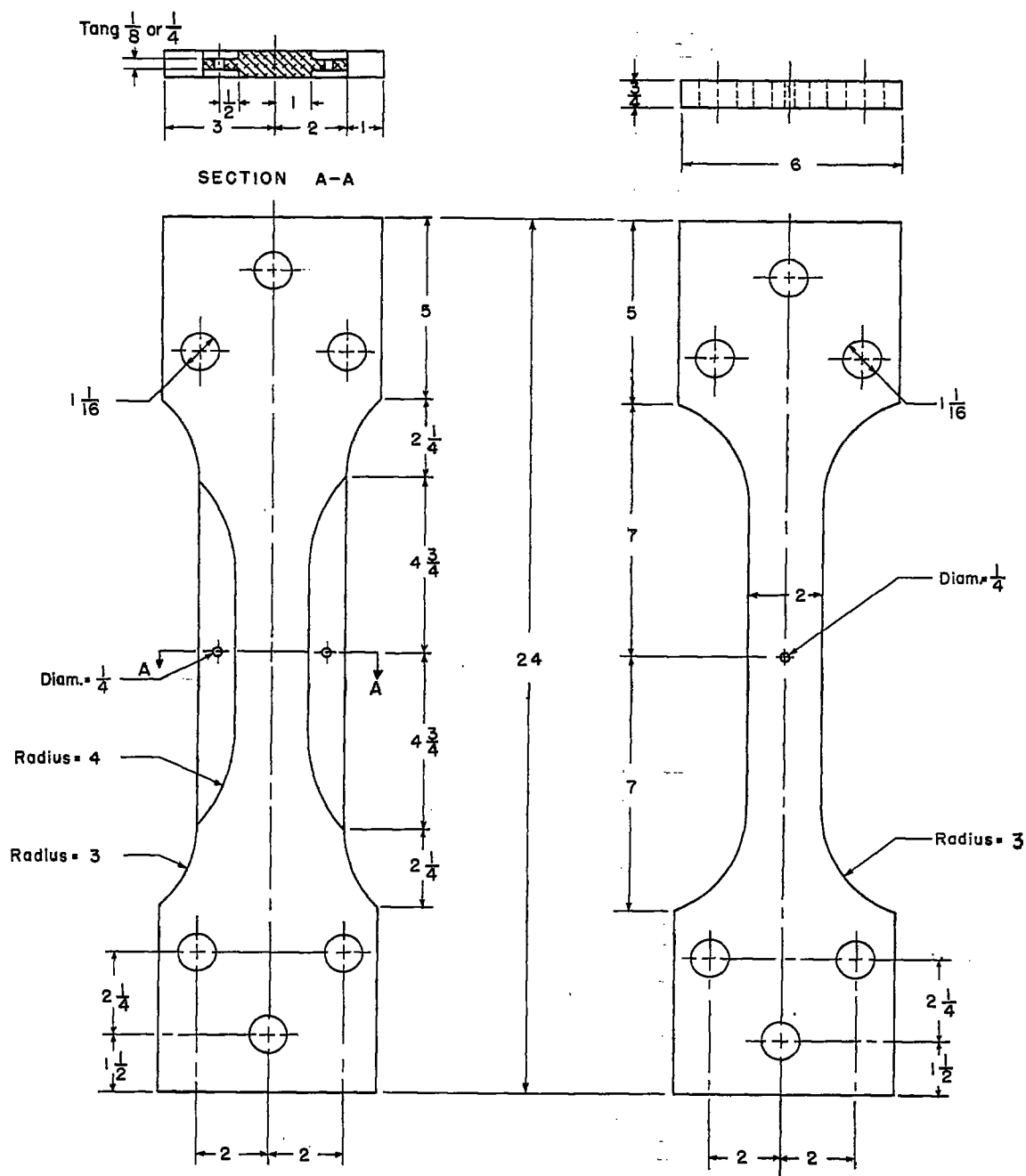


Figure 3.- Configuration of specimens made from $\frac{3}{4}$ -inch-thick bar stock.

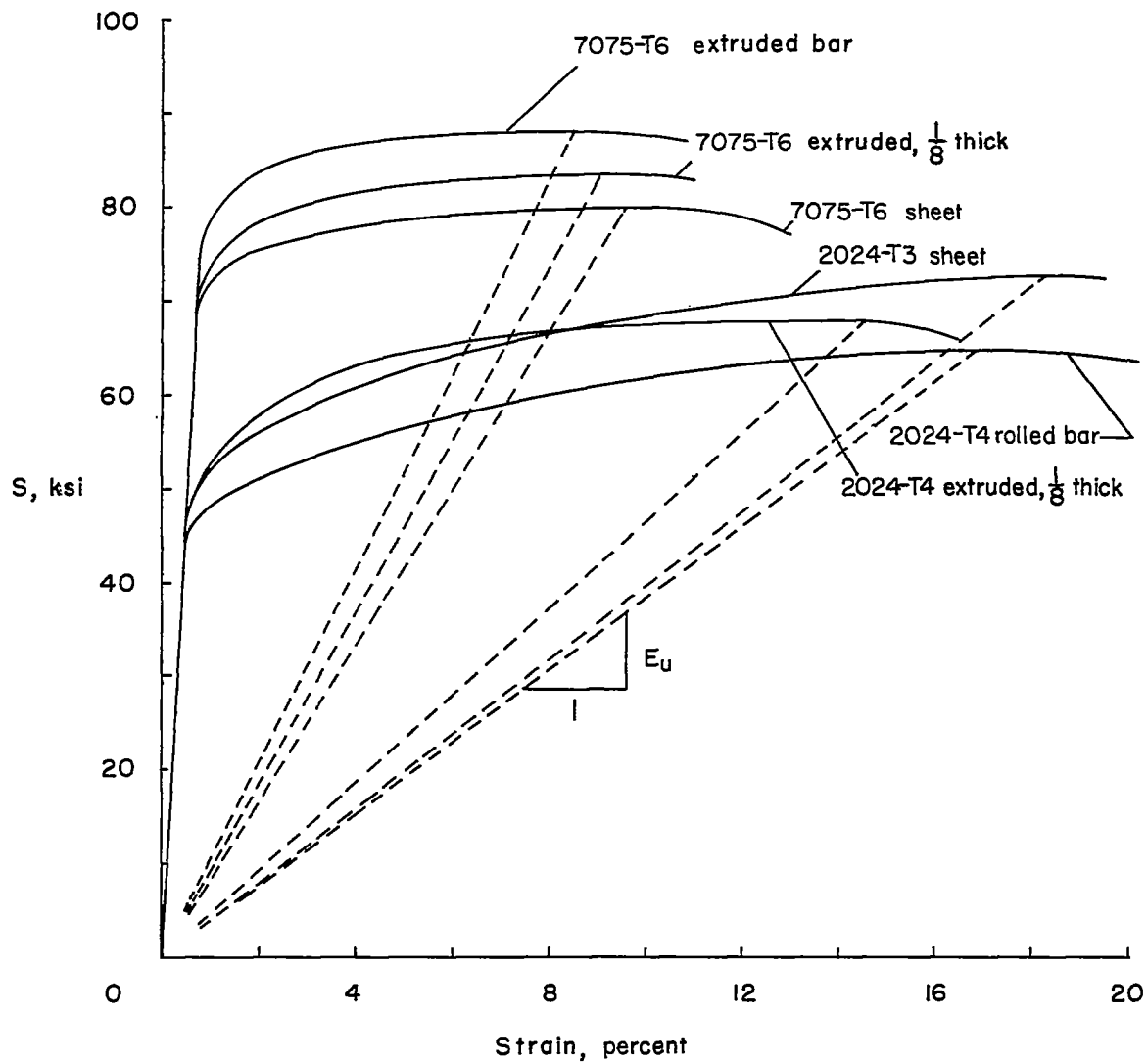


Figure 4.- Stress-strain curves for materials tested.

Face

Transverse

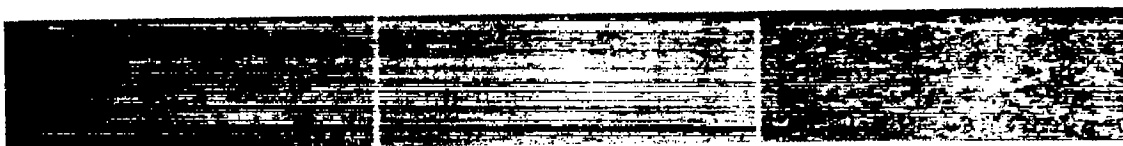
Longitudinal



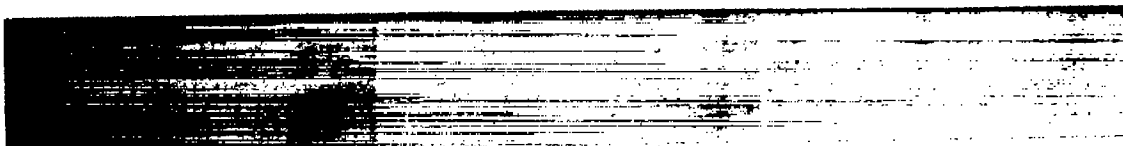
(a) 2024-T3 sheet.



(b) 2024-T4 extrusion.



(c) 7075-T6 sheet.



(d) 7075-T6 extrusion.

L-93582

Figure 5.- Macrostructure of materials used for small specimens ($\times 10$).

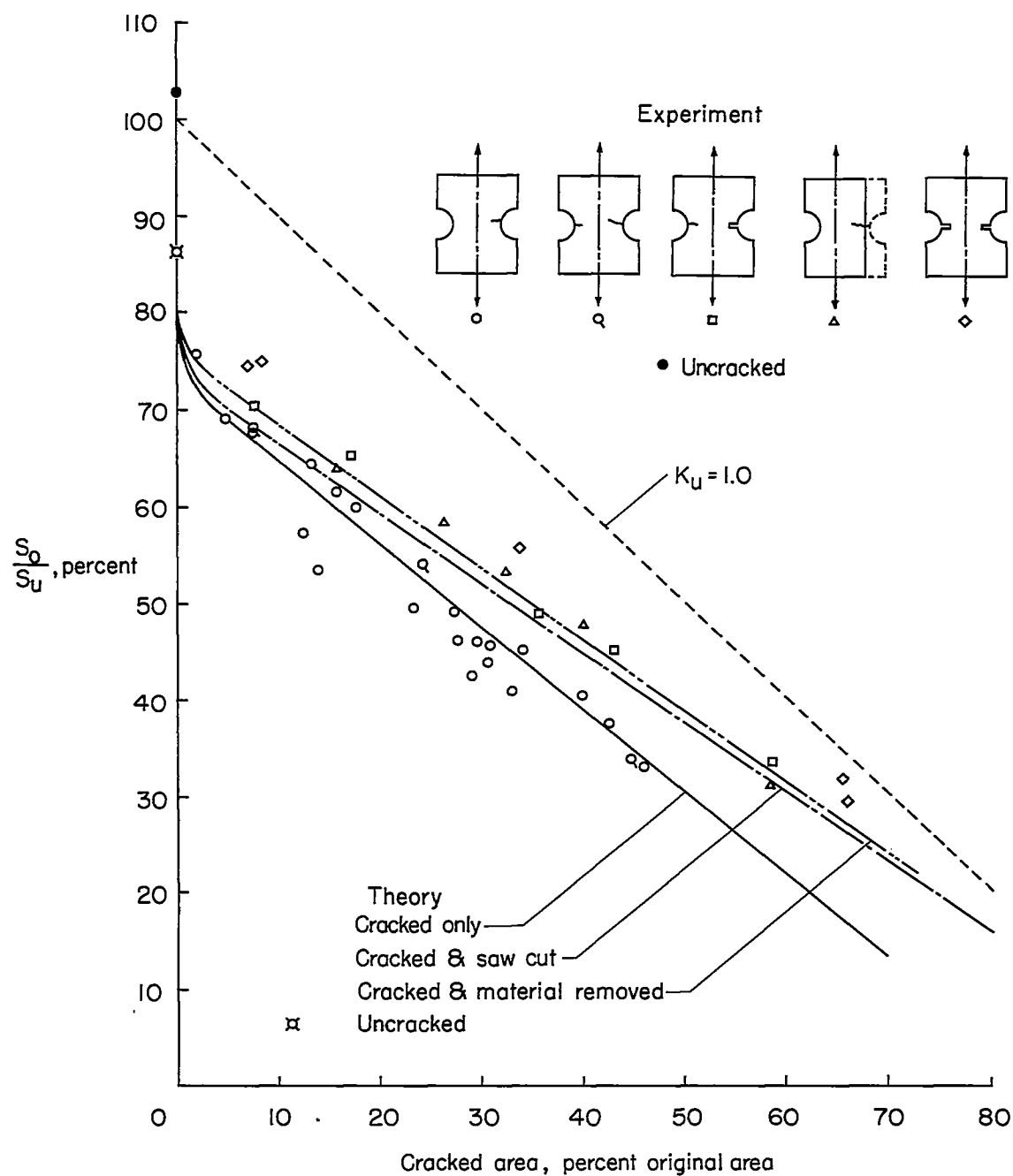


Figure 6.- Effect of fatigue cracks on strength of 2024-T3 aluminum-alloy-sheet specimens $2\frac{1}{4}$ inches wide.

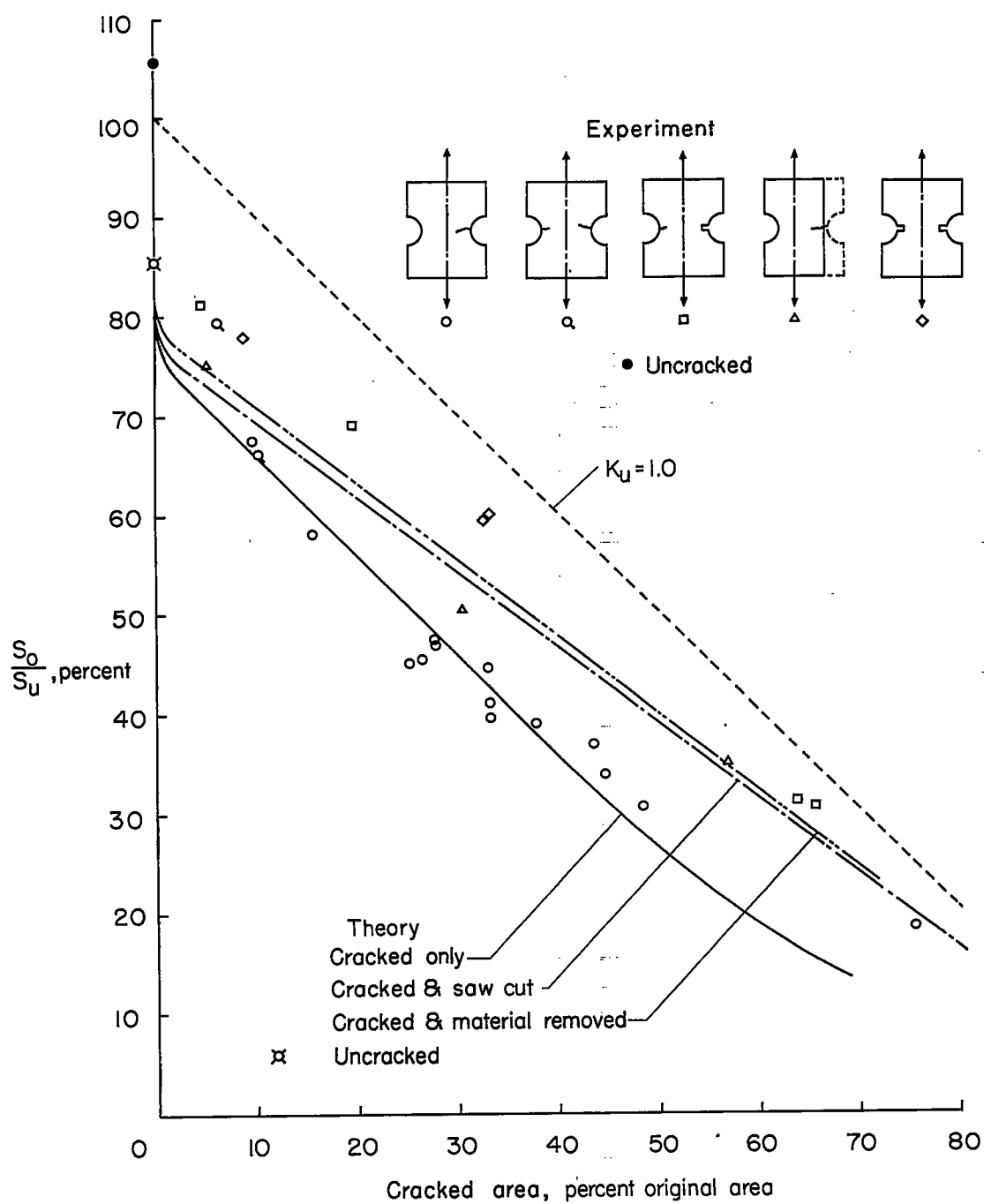


Figure 7.- Effect of fatigue cracks on strength of 2024-T4 aluminum-alloy-extrusion specimens $2\frac{1}{4}$ inches wide.

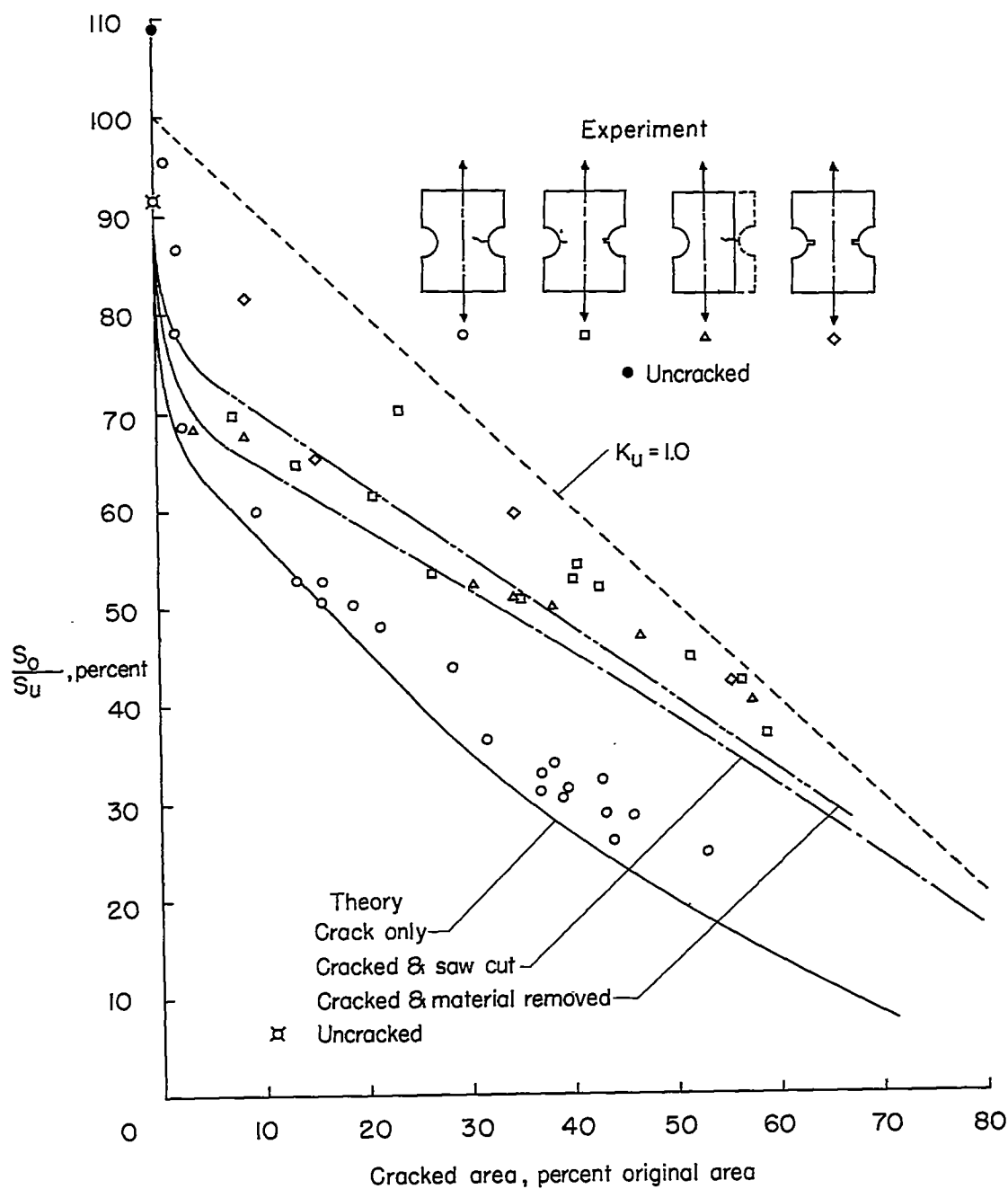


Figure 8.- Effect of fatigue cracks on strength of 7075-T6 aluminum-alloy-sheet specimens $2\frac{1}{4}$ inches wide.

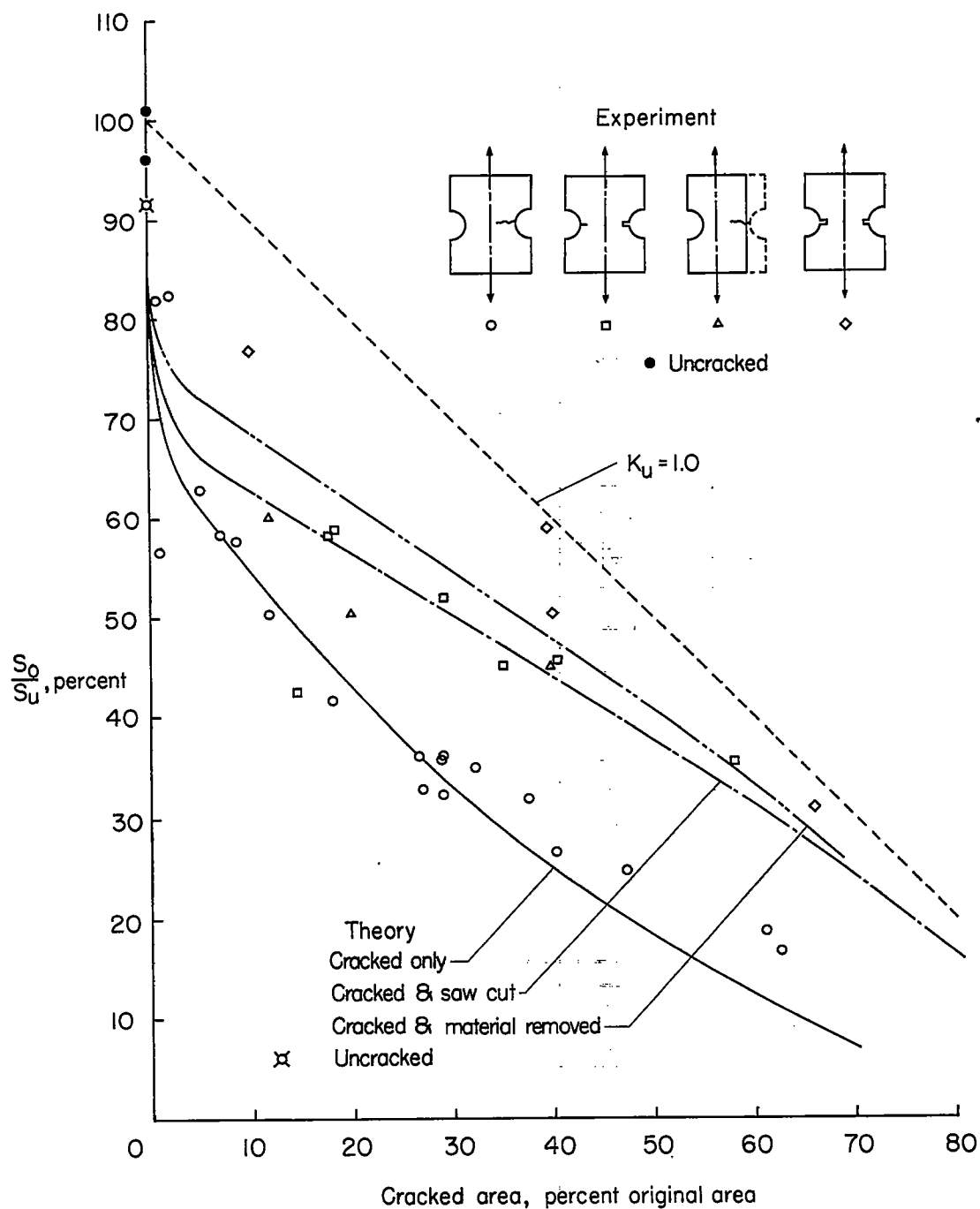


Figure 9.- Effect of fatigue cracks on strength of 7075-T6 aluminum-alloy extrusion specimens $2\frac{1}{4}$ inches wide.

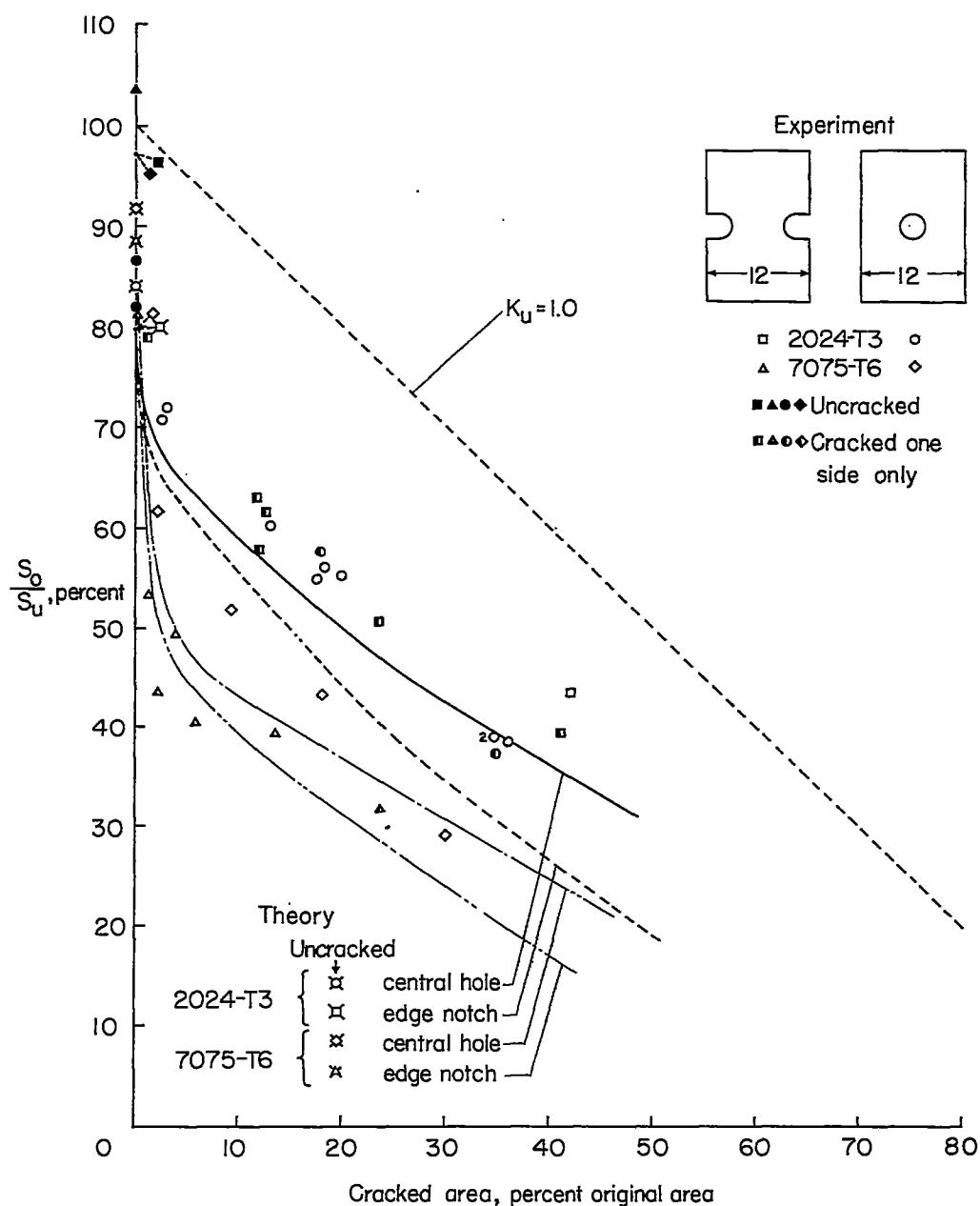


Figure 10.- Effect of fatigue cracks on strength of 2024-T3 and 7075-T6 aluminum-alloy-sheet specimens 12 inches wide. (Symmetrical cracks were assumed in computing curves for specimens with central holes; cracks on one side only were assumed in computing curves for specimens with edge notches.)

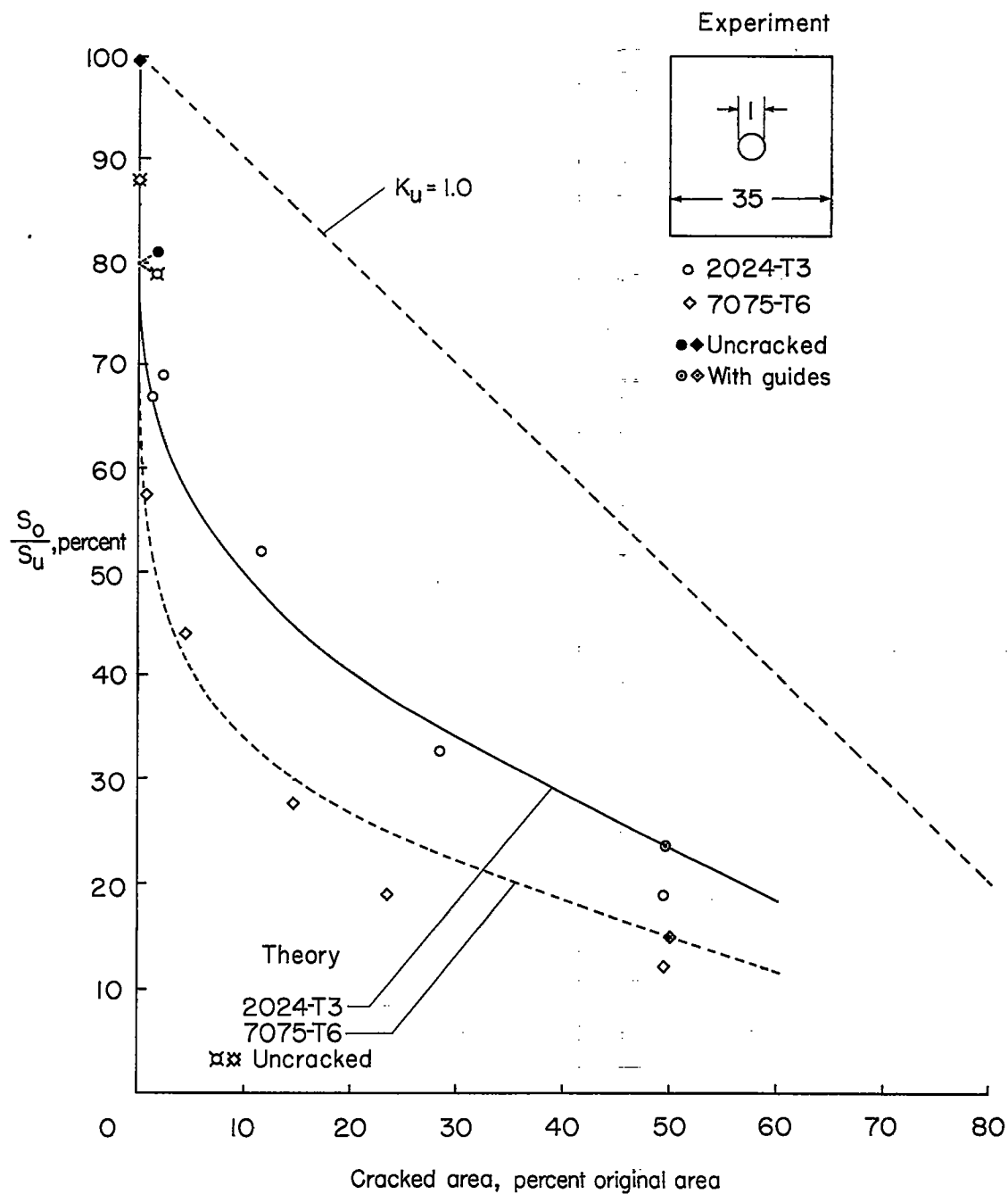


Figure 11.- Effect of fatigue cracks on strength of 2024-T3 and 7075-T6 aluminum-alloy-sheet specimens 35 inches wide.

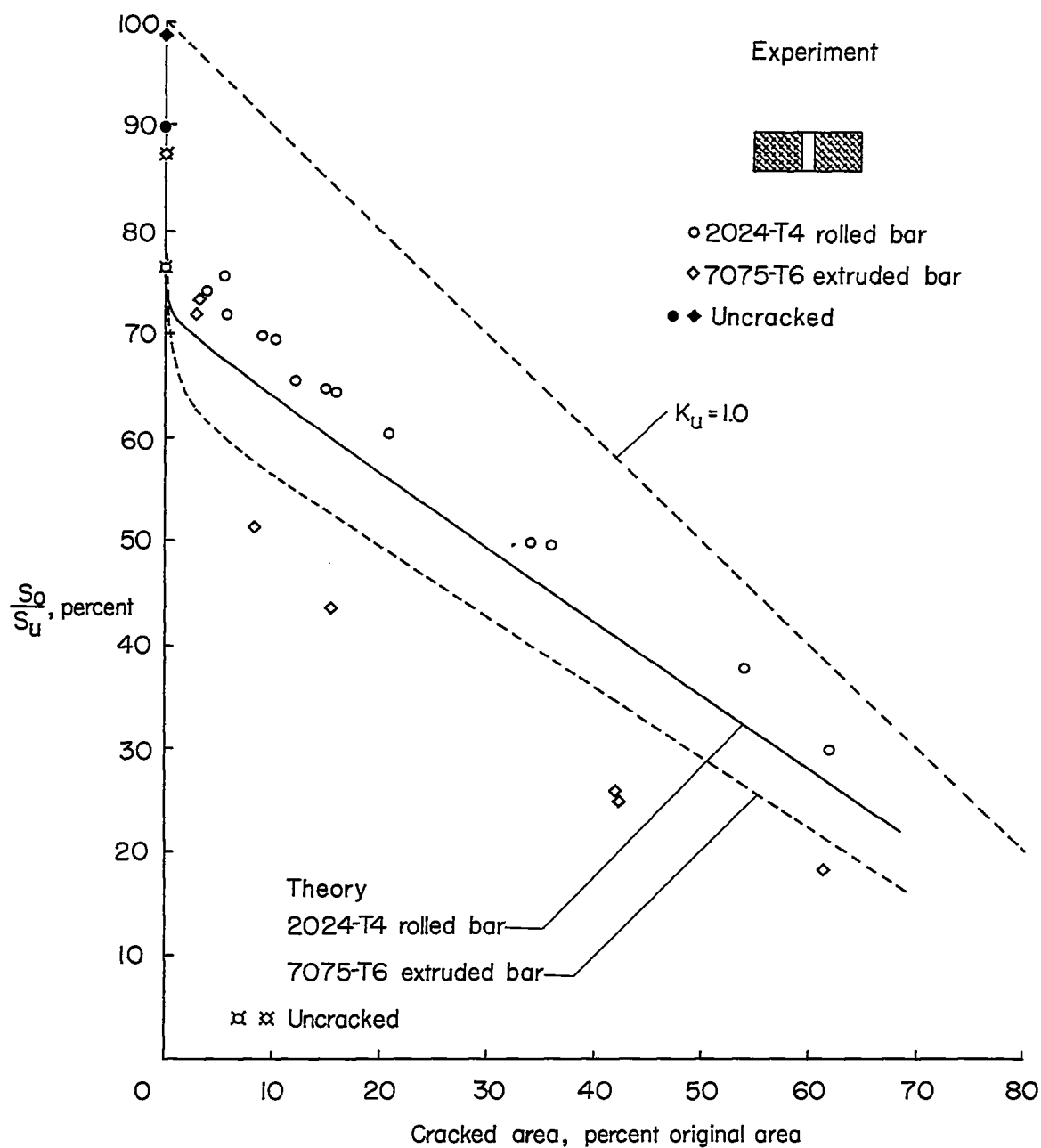


Figure 12.- Effect of fatigue cracks on strength of 3/4-inch-thick specimens made from 2024-T4 aluminum-alloy rolled bar and 7075-T6 aluminum-alloy extruded bar. (Symmetrical cracks were assumed in computing curves.)

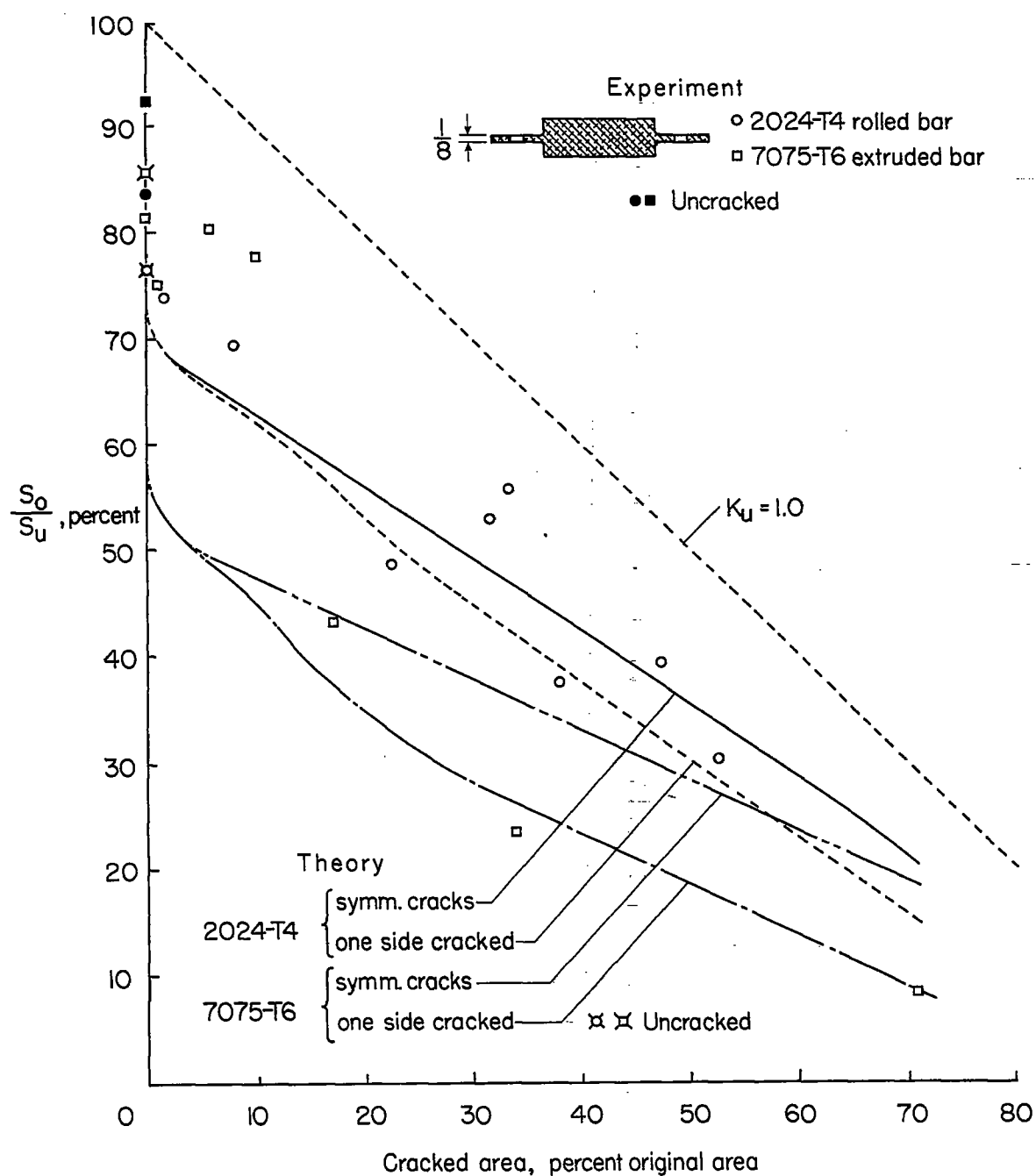


Figure 13.- Effect of fatigue cracks on strength of 1/8-inch-thick tang specimens made from 2024-T4 aluminum-alloy rolled bar and 7075-T6 aluminum-alloy extruded bar.

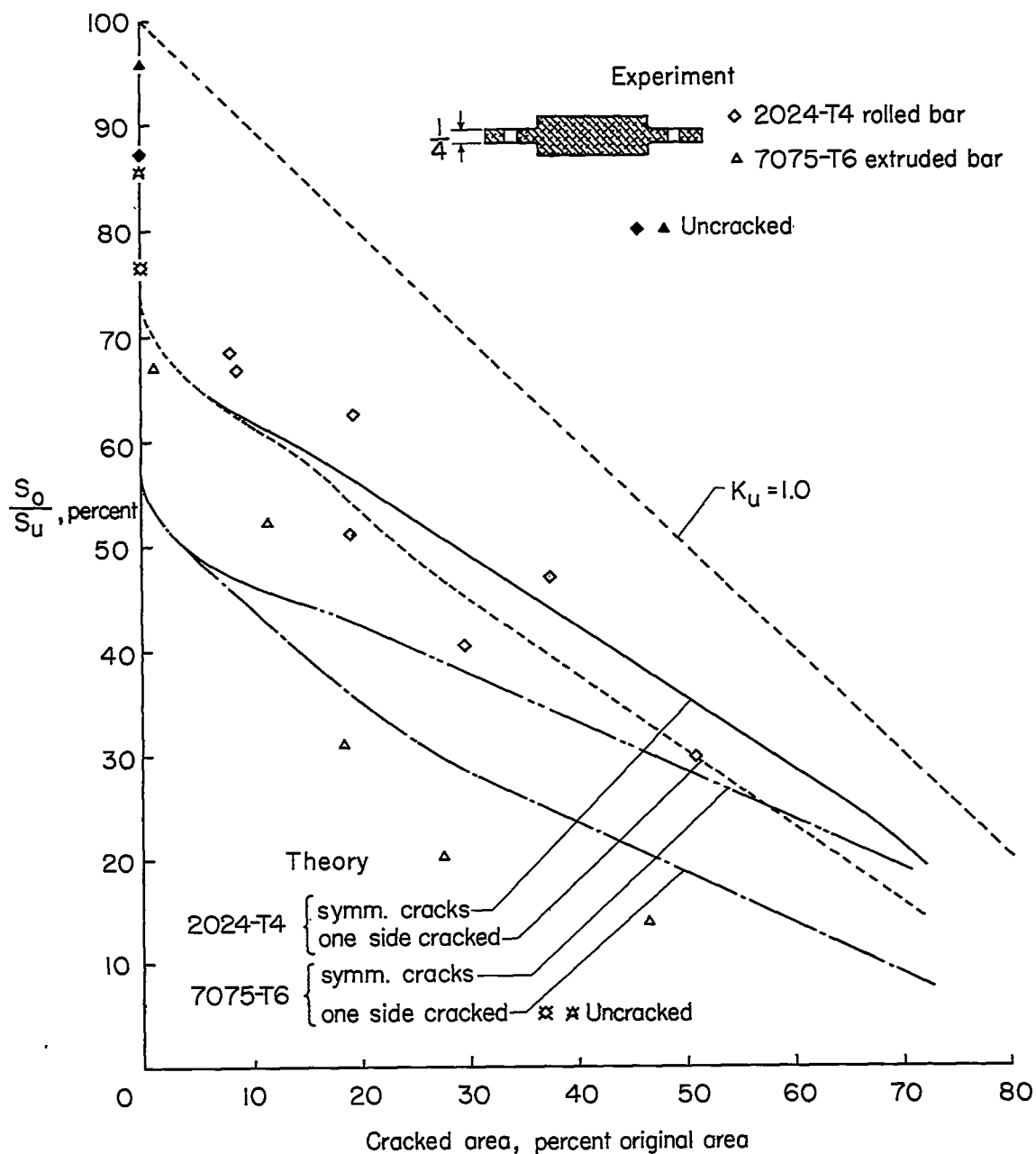


Figure 14.- Effect of fatigue cracks on strength of 1/4-inch-thick tang specimens made from 2024-T4 aluminum-alloy rolled bar and 7075-T6 aluminum-alloy extruded bar.

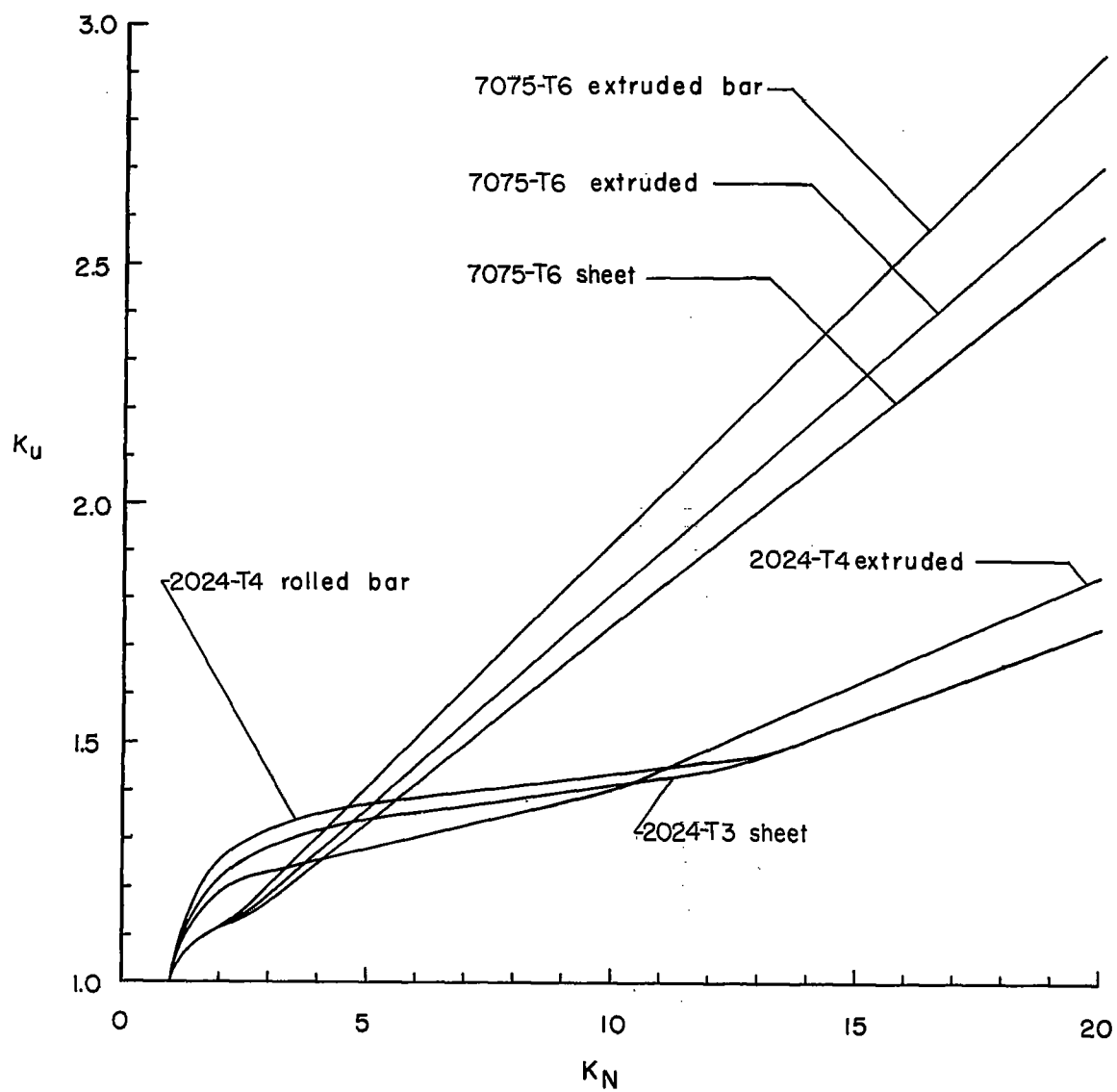


Figure 15.- Relation between stress concentration factor at failure and the Neuber factor.

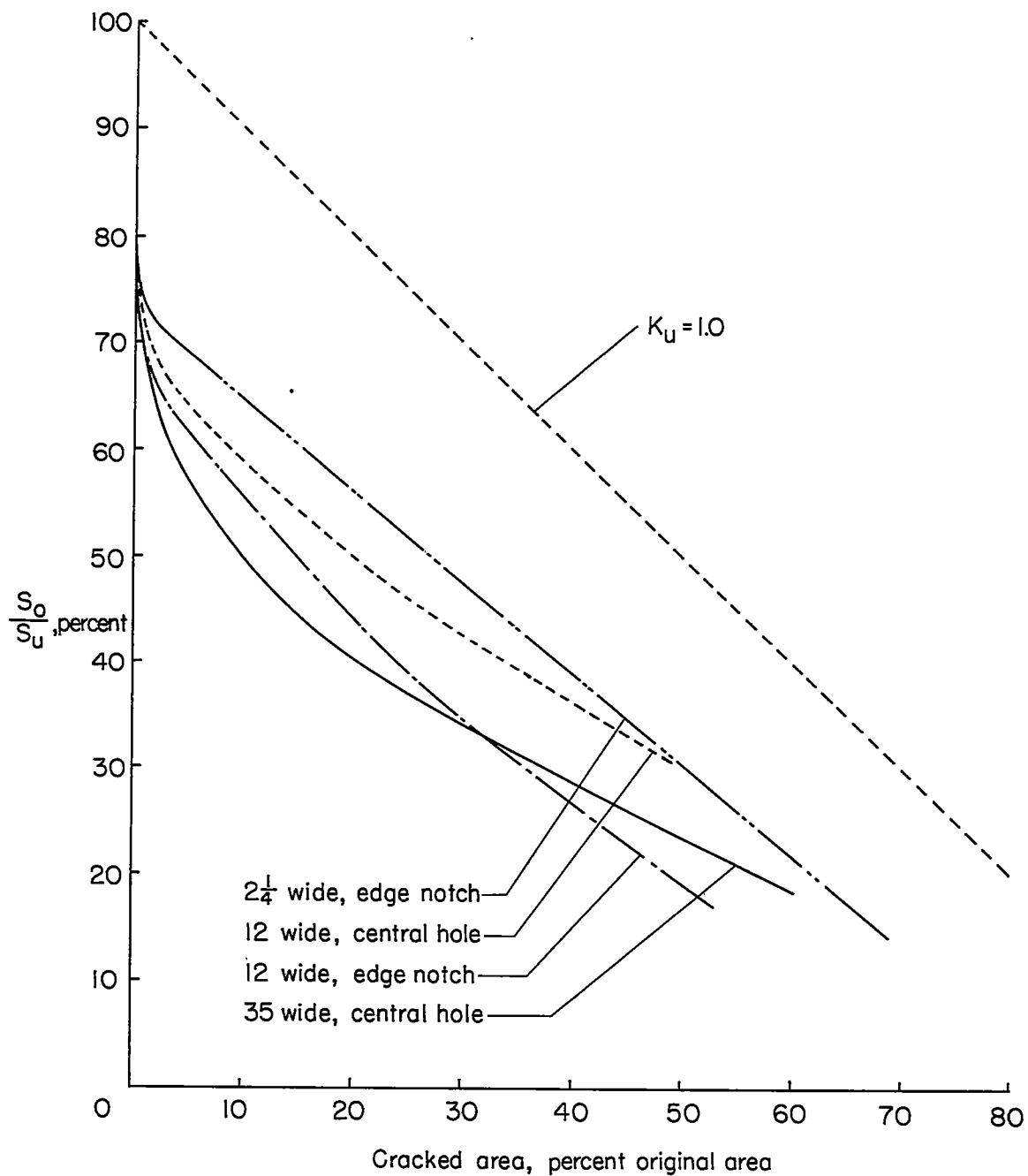


Figure 16.- Predicted strengths of 2024-T3 aluminum-alloy-sheet specimens. (Symmetrical cracks were assumed in computing curves for specimens with central holes; cracks on one side only were assumed in computing curves for specimens with edge notches.)

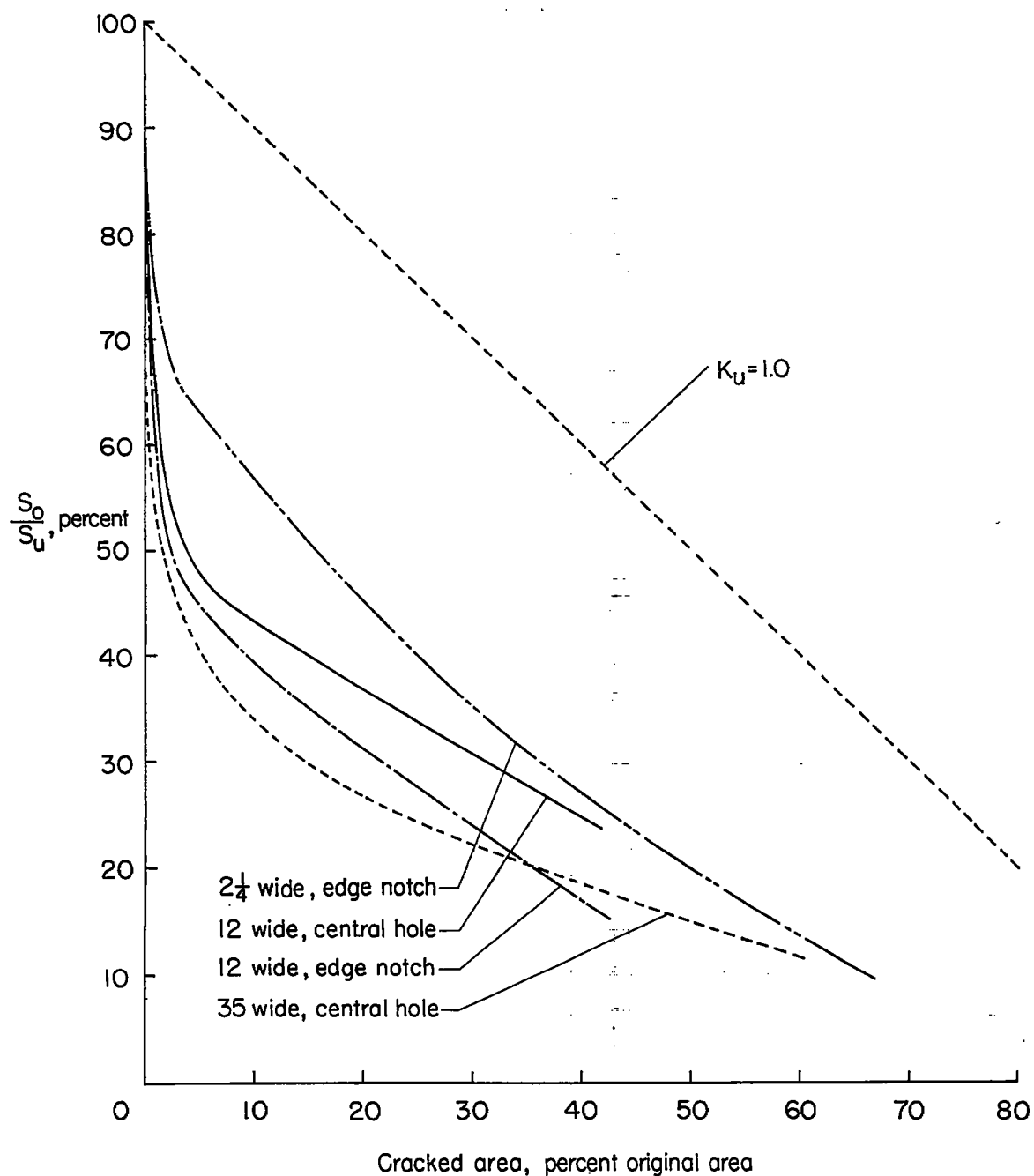


Figure 17.- Predicted strengths of 7075-T6 aluminum-alloy-sheet specimens. (Symmetrical cracks were assumed in computing curves for specimens with central holes; cracks on one side only were assumed in computing curves for specimens with edge notches.)

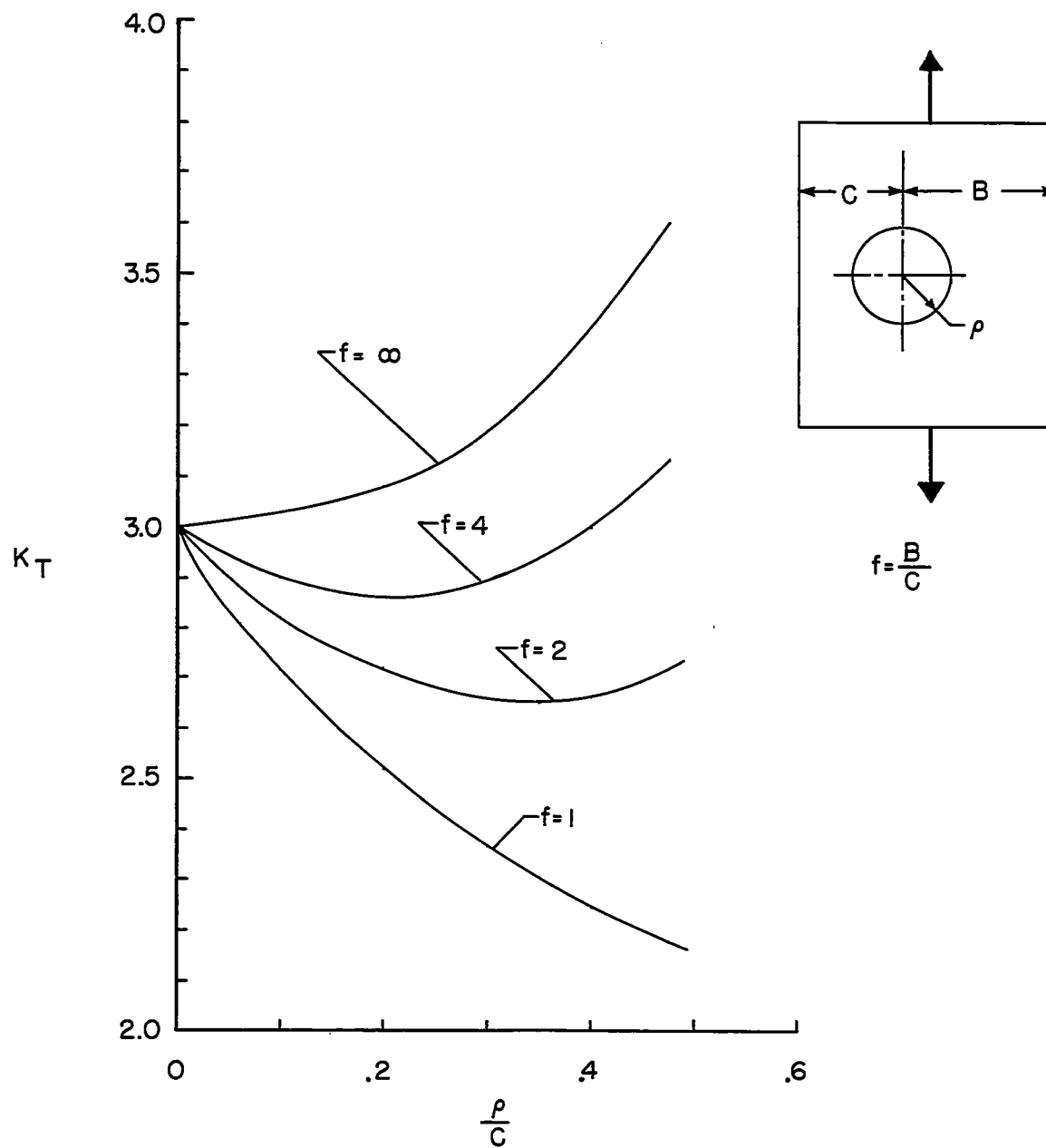
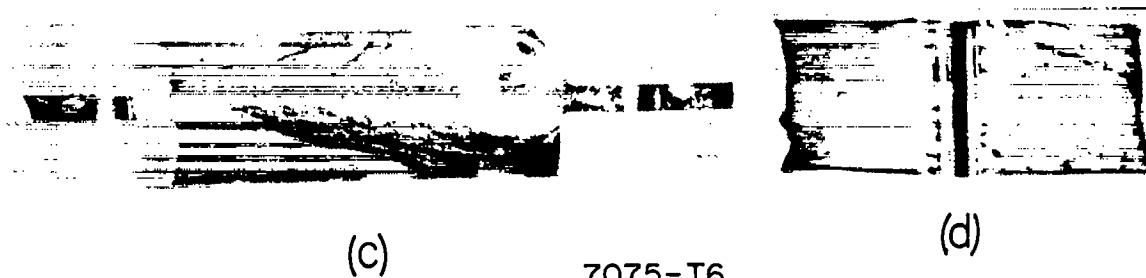


Figure 18.- Stress concentration factor for an axially loaded sheet containing an eccentric hole.



2024-T4
Rolled bar



7075-T6
Extruded bar

Figure 19.- Photographs of failed surface of 3/4-inch-thick specimens. L-93581